CARBON FILLERS FOR ACTUATION OF ELECTROACTIVE THERMOSET SHAPE MEMORY POLYURETHANE COMPSITES BY RESISTIVE HEATING

A Dissertation

by

YA-JEN YU

Submitted to the Office of Graduate and Professional Studies of
Texas A&M University
in partial fulfillment of the requirements for the degree of

DOCTOR OF PHILOSOPHY

Chair of Committee,	Duncan J. Maitland
Committee Members,	Melissa A. Grunlan
	Hung-Jue Sue
	Victor Ugaz
Head of Department,	Gerard L. Coté

May 2014

Major Subject: Biomedical Engineering

ABSTRACT

The shape memory polymer (SMP) is one type of smart material with shape memory effect. SMP's recovery can be actuated by external energy, such as heat. However, traditional direct heating limits potential applications of the SMP device. Thus, focusing on stimuli-responsive SMPs enables researchers to develop more versatile devices with SMP composites. The electroactive SMP composites incorporated with conductive fillers such as carbon black and carbon nanotubes allow shape recovery actuation by electrical resistive heating. Until now, most developments in electroactive SMPs are based on the use of a thermoplastic matrix doped with conductive fillers. Only limited reports have been made of thermoset polymers as the matrix used to synthesize an electroactive SMP composite.

In this study, thermoset SMP composites with loading carbon black and carbon nanotube are made and characterized by evaluating thermomechanical behavior, measuring electrical resistivity and percolation threshold, coating with water-resistant membrane, and actuating the device with resistive heating. The electrical conductivity of thermoset SMP composites will be investigated so that a voltage-triggered or resistive-heat-triggered shape memory polymer for applications where a self-actuated polymer is necessary. The development of electroactive SMP composites makes this research advantageous for electrical resistive heating of device design in minimally invasive surgery application.

ACKNOWLEDGEMENTS

I am grateful to my advisor, Professor Duncan J. Maitland, for his funding throughout my graduate studies and research. In addition to my advisor, I would like to thank the rest of my committee members, Professors Melissa A. Grunlan, Professor Hung-Jue Sue and Dr. Thomas S. Wilson, for their time in reviewing the papers and for their thoughtful advice and feedback. Also, I would like to thank of Dr. Victor Ugaz for his comments in my research.

I also thank my fellow labmates, Stephen Infanger, Keith Hearon, Dr. Brent Volk, Jennifer Rodriquez, Tony Boyle, John Horn, Todd Landsman and Mark Wierzbicki for my research. They also inspire me in research through our interactions and discussions in the lab.

Last but not the least, my deepest gratitude goes to my wife, Chia-Lan Liu, and my family; most especially, my wife who spiritually supported me throughout my pursuit of a higher education.

NOMENCLATURE

CB	Carbon black
CB1	1wt% carbon black
CB3	3wt% carbon black
CB4	4wt% carbon black
CB4.5	4.5wt% carbon black
CB5	5wt% carbon black
CB5/silicone-$_{Al2O3}$	CB5 coated with Al_2O_3-filled silicone
CB5/silicone-$_{silica}$	CB5 coated with silica-filled silicone
CB5$_{silicone-Al2O3}$	CB5 coated with Al_2O_3-filled silicone
CB5$_{silicone-silica}$	CB5 coated with silica-filled silicone
CB7	7wt% carbon black
CNT	Carbon nanotube
CNT1	1wt% carbon nanotube
CNT3	3wt% carbon nanotube
CNT3.5	3.5wt% carbon nanotube
CNT4	4wt% carbon nanotube
CNT4.5	4.5wt% carbon nanotube
CNT5	5wt% carbon nanotube
CNT5/silicone-$_{Al2O3}$	CNT5 coated with Al_2O_3-filled silicone
CNT5/silicone-$_{silica}$	CNT5 coated with silica-filled silicone

$CNT5_{silicone\text{-}Al2O3}$	CNT5 coated with Al_2O_3-filled silicone
$CNT5_{silicone\text{-}silica}$	CNT5 coated with silica-filled silicone
CNT7	7wt% carbon nanotube
CTE	Coefficient of thermal expansion
DMA	Dynamic mechanical analysis
DSC	Differential scanning calorimetry
HDI	Hexamethylene diisocyanate
HPED	*N,N,N',N'*-tetrakis(2-hydroxypropyl) ethylenediamine
MWNT	Multi-walled nanotube
NP	Neat polymer
ox-CNF	Oxidized carbon nanofiber
PCL	Poly(ε-caprolactone)
PTC	Positive temperature coefficient
PU	Polyurethane
R	Resistance of stretch specimen
R_0	Original resistance
SEM	Scanning electron microscopy
$Silicone\text{-}_{Al2O3}$	Al_2O_3-filled silicone
$Silicone\text{-}_{silica}$	silica-filled silicone
SMA	Shape memory alloy
SMP	Shape memory polymer
SWNT	Single-walled nanotube

TEA	Triethanolamine
T_g	Glass transition temperature
TGA	Thermal Gravimetric Analysis
T_m	Crystalline melt transition temperature
θ_{static}	Contact angle
ρ	Electrical resistivity

TABLE OF CONTENTS

Page

LIST OF FIGURES

Page

LIST OF TABLES

Page

CHAPTER I

INTRODUCTION

Currently, shape memory alloys (SMAs) are the most widely used shape-memory materials; however, these SMAs have some limitations [1]. At this time, many shape memory polymer (SMP) systems have been developed, and in comparison with SMAs, the SMPs have potential advantages. The raw material cost, density, fabrication charge, and processing of SMPs is less than that of SMAs [2]. The recoverable strain properties of SMPs are such that they can recover up to 100% of their prestrain extension [3]. The SMPs also blend easily with different fillers such as clay [4], nickel particles [5], carbon fibers [6], silicon carbide [7], and carbon nanotube [8], and carbon black [9] to change their thermomechanical properties. In addition, SMPs can be manufactured to respond to specific stimuli such as heat [10], light [11], electrical field [12], magnetic field [13], and moisture [14]. Due to the potential impact of biomedical devices that are capable of changing their geometries, numerous SMP-based devices are currently being investigated. One SMP-based suture anchor, Morphix®, has already been approved by the FDA in 2009 and is currently being implanted into patients' bodies.

Traditional thermoresponsive SMPs are heated above their transition temperature, deformed into secondary geometry, and subsequently cooled below their transition temperature to fix a secondary geometry. The secondary geometry is maintained because thermodynamic barriers prevent the polymer chains from relaxing and returning to their original state of higher entropy, which the chains automatically assumed during initial polymerization or processing. After heating above its transition

temperature, the deformed SMP returns to its high-entropy state, this is the primary geometry [3, 10, 15-17]. At the molecular level, netpoints such as covalent crosslinks and/or physical crosslinks enhance the integrity of the SMP system by keeping polymer chains from sliding past one another while the polymer is heated above its transition temperature [16]. Generally, the covalent crosslinks (thermoset SMPs) are more effective than physical crosslinks (thermoplastic SMPs), which can have better shape retention and recovery because of the excellent rubber elasticity above glass transition temperature [18].

Various fillers have been added to thermoplastic SMPs composites to derive multiple functionalities [19]. Liang *et al* [20] evaluated the deterioration of urethane-based SMPs that are chopped and woven fiberglass and unidirectional Kevlar® fibers. Ni *et al* [21] found that after adding 10 wt% chopped glass fibers, the elastic modulus of the urethane-based SMPs increased by 50%; however, the ratio of the shape memory recovery decreased to 25% from 60%. Li *et al* [9] investigated the composites of 20% carbon black and urethane-based SMPs with the crystallized PCL diol soft segments that decrease the electrical resistivity and increase the modulus; however, the recovery ratio decreases significantly. Cho *et al* [22] reported that urethane-based SMPs with added silica do not significantly change the recovery ratio but slightly increase the modulus. Gunes *et al* [6, 7] studied various nanofillers, such as clay, carbon nanofiber, silicon carbide, and carbon black, in urethane-based SMPs. They found that organoclay enhances the shape memory recovery. With an increase in added fillers of carbon nanofiber and silicon carbide, they reported that the recovery ratio gradually decreases.

Loading 5% carbon black into the matrix destroys the shape memory properties. Jimenez *et al* [23] found that the filler surface affects soft segment crystallinity and shape memory properties under urethane-based SMPs with PCL diol. Results of their studies showed that oxidized carbon fiber yields better dispersion, higher crystallinity, and better recovery ratio when compared with untreated carbon fiber filler. Paik *et al* [24] reported that the urethane-based SMPs with added fillers of carbon black and carbon nanotube increased the electrical resistance under elongation and decreased as more fillers were added. Cho *et al* [25] investigated the urethane-based SMPs with modified multiwall carbon nanotube by solution mixing and sonication, and they then demonstrated SMP actuation by Joule heating. Jung *et al* [26] studied the electroactive urethane-based SMPs with added carbon nanotubes, and treated with strong acid H_2SO_4/HNO_3 by conventional blending, in situ and crosslinking polymerization. Because polymers are typically considered insulators, heat transfer becomes the primary property that triggers these SMPs. For that reason, fillers have played an important role in assisting direct and indirect heating that improves thermal conductivity.

In the field of adding fillers to SMPs, research has focused on the nanoparticulate-filled system. The carbon nanotube and carbon black are the most popular fillers for doping into urethane-based SMPs matrix [19]. Today, there are two major carbon nanotubes types: single-walled nanotubes (SWNT) [27] and multi-walled nanotubes (MWNT) [28]. The SWNT structure contains one sheet of grapheme that rolls into a seamless cylinder with a 1-nm diameter and up to centimeters in length [27]. The MWNT structure consists of several separations in the basal plan of graphite, separated

by 0.35 nm, to form concentric cylinders. MWNTs are generally 2 to 100 nm in diameter and tens of microns in length [28]. Pristine carbon nanotubes are extremely conductive. Based on its 1D nature, charge carriers can travel through nanotubes without being scattered. The absence of scattering means that Joule heating is minimized so that carbon nanotubes can carry a large current density [29]; thus, carbon nanotubes function electrically as a metal or semiconductor. Also, the carbon nanotubes have excellent mechanical strength. In the high-quality SWNTs and arc-discharge MWNTs, their modulus and strength values can be upwards of 1 TPa to tens of GPa [30]. With suitable dispersion, nanotubes reinforce the matrix so that external stress applied to the matrix can be efficiently transferred to the nanotubes [31]. Carbon black forms from crystallographic structures that are stacked from three to four layers deep and every layer structure is composed of hexagonal carbon rings. Crystallites initially form primary particles and then form into primary aggregates [32]. Using carbon black as conductive fillers, particle size and structure are two important properties [33]. When carbon black is composed of a larger surface and higher porosity, it will more easily convey electrical conductivity at a lower percent filling of carbon black in a polymer composite. Thus, the separation distance between the carbon black aggregate is shorter than the critical distance; therefore, the electrons can easily transfer over the polymer barrier [34]. The loading concentration of conductive fillers reaches a quantity that causes a dramatic increase in electrical conductivity, which is called the percolation threshold [32, 35]. Below this concentration level, the filler particles are not interconnected in the matrix.

Once the filler concentration reaches the percolation threshold, the fillers can contact each other to form a conducting network.

Using the percolation concept, Kirkpatrick *et al* [36] showed that the electrical conductivity above the percolation threshold has following the relationship:

$$\sigma = \sigma_0(V - V_c)^s \quad (1)$$

where σ is the conductivity of the composite, σ_0 is the conductivity of the fillers, V is the volume fraction of the filler, V_c is the volume fraction of percolation threshold concentration, and s is the constant. Typically, in the 2D case, s is 1.1, and in the 3D case, s is between 1.5 and 1.6. Aharoni *et al* [37] and Janzen *et al* [38] developed a model of the mean number of contacts between fillers particles. They based their calculation results on Kirkpatrick's concept to acquire the 1.5 constant of the contact number and proposed the following equation:

$$V_c = \frac{1}{1+0.67z\rho\epsilon} \quad (2)$$

where V_c is the volume fraction of the percolation threshold, z is the coordination number, ρ is the density of the filler particles, and ϵ is the specific pore volume of the filler particles. Bueche *et al* [39] proposed using binary mixtures with the matrix and the conducting network, and concluded that the network chains functions as parallel conductors through the test sample. The following equation is based on those assumptions:

$$\frac{\rho}{\rho_m} = \frac{\rho_f}{(1-V)\rho_f + VW\rho_m} \quad (3)$$

where ρ is the mixture resistivity, ρ_f is the resistivity of the conducting network particles, ρ_m is the resistivity of the matrix, V is the volume fraction of conducting phase in the

mixture, and W is the fraction of the conductive filler. This model can explain the variations in conductivity when f is used as an adjustable parameter. Other than the models with the previous introductions, they are all used to explain the behavior of the percolation threshold [40, 41]; however, no single model explains the various experimental results.

Approaching the filler concentration of the percolation threshold, several models were based on assumptions that yielded the equations. Carbon black is not isolated in a dispersed manner but aggregated in the matrix because of Van der Waals forces. Generally, for a high-structure aggregate, each one is composed of 100–300 carbon black particles; for a low-structure aggregate, each one is composed of 30–100 carbon black particles. Based on the question of carbon black aggregate with no regular shape, Liang *et al* [42] various researchers used a number of assumptions to simplify the problem: (1) all individual carbon black diameter is represented by d, the volume of each aggregate is equivalent and is D_e in diameter, the number of carbon black particles per aggregate is N; (2) in the matrix, the equivalent aggregate randomly distributes itself and it can fill up the composites space completely. Based on these assumptions, the volume of equivalent sphere of carbon black aggregate, V_e, is as follows:

$$v_e = \pi D_e^3/6 \tag{4}$$

The expression for the overall volume of the carbon black particle in an aggregate, V_p, is given by the following equation:

$$v_p = N\pi d^3/6 \tag{5}$$

Based on asymmetric theory, conductive composites with doping carbon black are expressed in the following equation:

$$\varphi_l((\sigma_l - \sigma_m)/(\sigma_l - 2\sigma_m)) + \varphi_e((\sigma_h - \sigma_m)/(\sigma_h + 2\sigma_m))=0 \quad (6)$$

where φ_l is volume fraction of low-conductivity components, φ_e is volume fraction of the equivalent sphere, σ_m is the electric conductivity of composites, and σ_l and σ_h are the conductivity of low–conductivity and high-conductivity components, respectively. The insulator-conductor transition will occur when $\varphi_e$is equal to 1/3. Furthermore, v_e and v_p are different and on this basis, the following expression results:

$$\frac{v_e}{v_p} = \frac{\varphi_e}{\varphi_p} = \frac{D_e^3}{Nd^3} \quad (7)$$

where φ_p is the volume fraction of carbon black. The conductivity of the composites is obtained by solving Eqs. (6) and (7) and is expressed by the following equation:

$$\varphi_l((\sigma_l - \sigma_m)/(\sigma_l + 2\sigma_m)) + \varphi_p D_e^3((\sigma_h - \sigma_m)/(\sigma_h + 2\sigma_m))/Nd^3=0 \quad (8)$$

If σ_l =0, the percolation threshold of the conductive composites with doping carbon black is expressed as:

$$\varphi_{pc} = Nd^3/3D_e^3 \quad (9)$$

To determine the percolation threshold in a fiber system, Berhan *et al* [43] developed that the model is based on interpenetrative rigid spherocylinders, randomly in three dimensions. These "sticks" are assumed to be straight cylinders of *L* in length, *R* in radius, and *R* in radius of hemispheric end caps. For the assumptions, the number of objects per unit volume at percolation q_p is inversely proportional to the excluded volume V_{ex} of one of the objects as given by the following equation:

$$q_p \propto \frac{1}{v_{ex}} \tag{10}$$

The excluded volume for a given object is defined as that volume surrounding and including a given object, which is excluded by another object. Generally, for spherocylinders of length L and radius R , the excluded volume is as follows:

$$v_{ex} = \frac{32\pi}{3} R^3 \left[1 + \frac{3}{4}\left(\frac{L}{R}\right) + \frac{3}{8\pi}\langle sin(\theta)\rangle \left(\frac{L}{R}\right)^2\right] \tag{11}$$

where $\langle \sin(\theta) \rangle$ is the average of $\sin(\theta)$ for two sticks and θ is the angle between them. For a random distribution, $\langle \sin(\theta) \rangle = \pi/4$, thus:

$$v_{ex} = \frac{32\pi}{3} R^3 \left[1 + \frac{3}{4}\left(\frac{L}{R}\right) + \frac{3}{32}\left(\frac{L}{R}\right)^2\right] \tag{12}$$

The volume of a single spherocylinders is as follows:

$$v = \frac{4\pi}{3} R^3 + \pi R^2 L \tag{13}$$

For the very high-aspect ratio fibers ($R/L \rightarrow 0$), the analytical solution for q_p is often expressed as follows:

$$q_p = \frac{1}{v_{ex}} \tag{14}$$

Because q_p is the number of objects per unit volume at percolation, the analytical solution for the volume fraction of high-aspect ratio fibers at the percolation threshold is often expressed as:

$$\varphi_c = \frac{v}{v_{ex}} \tag{15}$$

However, this is the ideal condition to approach the percolation threshold in the 3D fiber system. In actual conditions, the carbon nanotube can easily aggregate and bundle itself

together because of strong Van der Waals forces. Carbon black and carbon nanotubes are both able to be dispersed within the polymer matrix.

Improvement of carbon filler dispersion in the matrix can achieve better reinforcing effect and electrical properties. Currently, there are various methods that have been examined in an effort to improve carbon filler dispersion in the polymer matrix [19, 31, 32]. The following methods have been evaluated.

a) Non-covalent functionalization—The surfactant, which does not compromise the physical properties of carbon fillers nor will it damage their structure, functions as micelles to surround the carbon fillers [44, 45]. Islam *et al* [46] determined that three major parameters, alkyl chain length, head group size, and charge, allow for the interaction between the surfactant and the carbon nanotube. One potential disadvantage of non-covalent bonding of the surfactant is that the force might become weaker between the carbon fillers and the network polymer.

b) Covalent functionalization—Adding functional groups such as -COOH and -OH are created on the carbon filler surfaces during the oxidation process by acid liquid treatment [47-49]; however, the treatment will damage the filler surface structure and physical properties. The presence of the carboxylic acid group on the carbon filler surface is easily transferred to other chemical reactions as another functional group or graft [44]. The modified carbon fillers can enhance their dispersion in the solvent and polymer matrix [50].

c) Solution mixing—Fillers dispersed in a solvent and polymer matrix are mixed in solution and the composites are then made by evaporating out solvent. Recently,

Sahoo *et al* [44] successfully added MWNT fillers up to 20%, well dispersed in a polyurethane matrix; however, the polymer matrix needs to dissolve in at least one type of solvent. Many polymers cannot meet this requirement.

d) Melt mixing—Specific for thermoplastic polymers, fillers are mechanically dispersed and mixed in a polymer matrix under high temperature and high shear force [7]. Gunes *et al* [6] prepared the thermoplastic urethane-based SMPs with carbon black using a chaotic mixer. Gunes *et al* [6] mentioned that using chaotic mixing easily let SMP composites achieve the electrical percolation at lower carbon filler content.

e) In situ polymerization—For this polymerization method, the fillers are dispersed in the monomer and followed by polymerization [44, 51, 52]. Jung *et al* [26] showed that the carbon nanotube with acid treatment can be used to form urethane-based SMPs. Their shape memory recovery can approach 96%, which surpasses the 87% shape memory recovery with the solution mixing process. Generally, in situ polymerization can be used for preparing composites that cannot be processed by solution mixing, melt mixing, insoluble polymer, and thermally unstable polymers. Depending on the polymer and filler type, different process designs based on their polymer's physical and chemical properties are considered in selecting the best way to disperse the carbon filler in the polymer matrix.

Polymers such as silicone rubber have been applied in membrane coatings on medical device surfaces [53, 54]. Silicones have wide applications in health care because of their biocompatibility and biodurability [55]. The silicone's biocompatibility is due to a lack of toxic degradation products from its relative purity, high-molecular-weight

polymeric nature, and chemical structure. The medical device application of silicone's biodurability is related to its thermal and chemical stability properties. Silicon has unique material properties such as high hydrophobicity, low surface tension, and chemical and thermal stability. Due to its inertness, silicone has been evaluated for applications in orthopedics, drains, shunts, extracorporeal equipment, and aesthetic implants.

The process of in situ polymerization is our method of choice for developing the electroactive shape memory of carbon-filled polyurethane composites. In situ polymerization is especially useful for dispersing fillers in the matrix and can overcome the limitations that some SMPs, such as thermoset polymers, which cannot be processed by the previously mentioned methods. Polyurethane can incorporate the two conductive nanoparticles—carbon black and carbon nanotube—to generate conductive networks among the SMP matrix. With suitable dispersion, the fillers in the polymer matrix connect together to approach the percolation threshold that increases the electrical conductivity. Thus, by applying voltage to initiate resistive heating in the SMPs, the SMP can return to its primary shape from its fixed secondary shape. For implant applications, a membrane coating is applied to the device, not only for biocompatibility and biodurability, but also to avoid current and filler leakage from the device into the body. To date, all studies on electroactive fillers in SMPs have been focused on thermoplastic SMPs systems; however, their poor thermal and mechanical properties cannot compare to thermoset SMPs. To the best of our knowledge, the limited studies of thermoset SMP composites with filler loading, such as that of Leng *et al* [5, 56-58], have

only used commercial thermoset styrene-based SMPs resin (CRG Industries, Veriflex®) and added nanocarbon powder to study their electrical property of SMP composites. Liu *et al* [59] loaded SiC into epoxy system to reinforce the matrix and measure their thermomechanics behavior, and Yakacki *et al* [60] incorporated Fe_3O_4 magnetite into acrylate-based system to remotely heat the SMP composites via exposure to an magnetic field. However, Wilson *et al* [61] have already developed a novel thermoset urethane-based SMP (neat polymer made from hexamethylene diisocyanate (HDI), N,N,N',N'-tetrakis(2-hydroxypropyl) ethylenediamine (HPED), and triethanolamine (TEA). Owing to the complexity of this process, adding the filler into a polymeric system is a challenge. This study aims to develop an understanding of the combination of thermoset urethane-based SMPs with added conductive fillers of carbon black and MWNT, and then apply the composite SMPs in evaluating the thermal, mechanical, and electrical properties of these materials as desired for their applications as a potential medical device.

CHAPTER II

THERMOSET SHAPE MEMORY POLYURETHANE COMPOSITES WITH CARBON FILLERS - PART I

2.1 Overview

Novel urethane thermoset shape memory polymer (SMP) composites with carbon black and carbon nanotube loading fillers have been synthesized and characterized. The addition of carbon nanoparticles to SMP has the potential to increase stress recovery. Many SMP composites focus on thermoplastic systems because of the processing challenges associated with thermoset production. Few thermoset SMP composite systems have been reported in the literature, which is the focus of our study. In Part I we found that carbon nanotubes were found to be more effective than carbon black for reinforcing the SMP matrix. The composites with carbon nanotube had lower strain recovery when compared to that of carbon black. Recovery also decreased when subjected to high pre-strain. Also, increasing the loading of the carbon fillers into SMP matrix shifts the glass transition temperature to lower value. In Part II we focused on the effect of carbon black and carbon nanotube for actuation of electroactive thermoset SMP composites by resistive heating.

2.2 Introduction

Shape memory polymers (SMPs) are stimuli-responsive smart materials whose unique ability to store a temporary geometry or geometries and actuate to a primary geometry has drawn attention from a wide array of industries, ranging from the aerospace and biomedical engineering industries to the culinary and commodity device industries [3, 62, 63]. One advantage of SMPs over other shape memory materials such

as shape memory alloys (SMAs) is higher recoverable strain capacity. Recoverable strains greater than 800% have been reported for certain SMPs, while those of SMAs have generally been reported to be in the range of 5% to 10% [64]. Other advantages of SMPs include lower moduli for improved environmental compliance matching in certain soft tissue applications, lower costs of production and processing, and facile tailor-ability of thermomechanical properties to meet highly specific material demands for various applications [15]. Thermally actuated SMPs can be heated above a thermal transition temperature, T_{trans}, deformed from a primary geometry into a desired secondary geometry while above T_{trans}, and then cooled below T_{trans} to fix this secondary geometry. Re-heating above T_{trans} enables actuation from the secondary geometry to the primary geometry [10, 65, 66]. T_{trans} can be a glass transition (T_g), a crystalline melt transition (T_m), or another thermal transition [67]. In addition to being thermoresponsive, SMPs can also be manufactured to respond to other stimuli such as light [11], electric fields [12], magnetic fields [13], or moisture [68].

The relatively low moduli of polymeric materials in comparison with those of metals and ceramics can at times be a material disadvantage instead of an advantage when higher stiffness or recovery stress is desirable. One method of increasing the moduli and recovery stresses of SMPs has been to blend SMP resins with fillers such as clay particles [4], nickel particles [5], carbon fibers [6], silicon carbide [7], carbon nanotubes [8] or carbon black [9] to create higher-modulus SMP composites. In these previous studies, it has often been shown that a tradeoff exists between filler composition and recoverable strain capacity [2]. Li *et al* [9] investigated the physical and

thermomechanical properties of polyurethane SMP composites containing crystallizable poly(ε-caprolactone) (PCL) soft segments and carbon black concentrations of up to 20 wt%. In Li's study, recoverable strain was shown to decrease significantly with increasing carbon black filler composition. Gunes *et al* [6, 7] investigated the effects of nanofillers such as clay, carbon nanofibers, silicon carbide, and carbon black on recoverable strain in polyurethane SMPs. Organoclay was shown to enhance recoverable strain capacity, carbon nanofibers and silicon carbide were shown to gradually decrease recoverable strain capacity, and carbon black was shown to significantly decrease recoverable strain capacity with 5% loading.

Many SMP composite studies have focused on polyurethane SMP systems because of the high versatility of polyurethanes, including high toughness, good biocompatibility for certain polyurethanes, and commercial availability of certain PU resins. Although a wide array of fillers have been reported in these previous studies, a much less diverse set of polyurethane matrices have been characterized, with a significant majority of these matrices being thermoplastic polyurethane matrices. Comparatively fewer studies have reported the synthesis and characterization of thermoset SMP composites. One potential reason for this weighted focus is the difficulty associated with the synthesis and mixing technologies required to synthesize thermoset SMP composites. Thermoset materials have sometimes been shown to have certain distinct advantages over thermoplastic materials, including better cyclic shape memory behavior, higher recoverable strains, and higher recovery stresses, especially during cyclic shape memory testing. Composite SMPs reported in the literature include one system made from a commercially available

thermoset styrene-based SMP resin with added fillers [21-23], an oligo(ε-caprolactone)dimethacrylate/butyl acrylate thermoset matrix containing magnetite nanoparticles [24], a commercial thermoset SMP epoxy system with added SiC particles [25], and a methacrylate-based thermoset SMP with added Fe_3O_4 magnetite particles [26].

In this study, we report the synthesis and characterization of a thermoset polyurethane SMP composite system based on the chemical formulations reported by Wilson *et al* [27] in 2007. This polyurethane SMP system is a single phase amorphous thermoset that has been shown to have excellent shape memory properties, including sharp glass transition regions, good cyclic recoverable strain behavior, and high percent recoverable strains. Specifically, we aim to determine the effects of carbon black and multi-wall carbon nanotube fillers on the polyurethane SMP matrix's physical properties. To overcome the synthetic challenges associated with the fabrication of thermoset SMP composites, we report a custom monomer/filler blending process and a curing process developed in-house. We also report the characterization of these SMP composites by dynamic mechanical analysis, tensile testing, and shape memory characterization experiments to illustrate the effects of filler loading on modulus, ultimate tensile properties, and recoverable stress and strain.

2.3 Experimental

2.3.1 Material synthesis and sample preparation

All monomers and fillers were used as received without further purification. The polyurethane SMP matrix was prepared from the trifunctional polyol triethanolamine

(TEA; Sigma Aldrich, 99%), the tetrafunctional polyol N,N,N',N'-tetrakis(2-hydroxypropyl) ethylenediamine (HPED; TCI America, 98%), and hexamethylene diisocyanate (HDI; TCI America, 98%) using a 0.133 : 0.4 : 1 mole ratio of TEA : HPED : HDI. The fillers used were carbon black (CB; Ensaco 250, primary particle size ~40 nm, soft granule size ~200 nm to 2 mm, density 0.17 g cm^{-3}, surface area 65 m^2 g^{-1}), and multi-wall carbon nanotubes (CNT; Sigma Aldrich 659258, 90%, residual amorphous carbon (metal contaminants, mostly iron, amount to less than 0.1%), dimensions 110-170 nm x 5-9 μm (diameter * length), density 1.7 g cm^{-3}, surface area 1.3 x 10^2 m^2 g^{-1}). The fillers were first dispersed in the viscous monomer HPED in 1, 3, 5, and 7 wt% ratios (overall final polymer mass) using a FlackTek™ SpeedMixer™ DAC 150 speed mixer at 3400 rpm for 0.5, 1, 1.5, and 2 min. The HPED/filler dispersions were then blended with TEA and then finally with HDI using the same speed mixer settings. The SMP composite was cured at room temperature for 120 min and then heat treated to polymerize at 120°C for 60 min and then slowly cooled down to room temperature. Finally, SMP composite was polished by computer numerical control (Roland MDX-540) into 1~1.5 mm in thickness.

2.3.2 Characterization

2.3.2.1 Dispersion

SMP composites containing varying CB and CNT filler composition were machined to 10 x 10 x 3 mm specimen dimensions, mounted in wax, and sliced using a Spencer 820 microtome. The specimens were then cut to 10 μm thicknesses. The surface

morphology and filler dispersion of SMP composites were analyzed using a Zeiss Axiovert 200 microscope in accordance with ASTM standard D2663-08. Dispersion was calculated using Equation (1),

$$Dispersion, \% = 100 - SU/L \quad (16)$$

where U is the number of graticule squares that are at least half filled (each square on the graticule is 10 by 10 μm), L is the volume percentage of filler in the compound, and S is swell factor. From every SMP composite ten images were analyzed and their values averaged.

2.3.2.2 Glass transition temperature

Differential scanning calorimetry (DSC) experiments were performed on 5-10 mg samples using a TA Instruments Q200 differential scanning calorimeter using a heat-cool-heat cycle repeated 3 times. Samples were heated from 40° to 150°C at 10°C/min, held isothermally at 150°C for 2 min, cooled to -40°C at 10°C/min, and held isothermally 2 min at -40°C. Two more heat-cool-heat cycles were then run on each sample. The data were recorded using TA Instruments Q Series™ software and analyzed using TA Instruments Universal Analysis software.

2.3.2.3 Storage modulus

Dynamic mechanical analysis (DMA) experiments were performed in tension using a TA Instruments Q800 dynamic mechanical analyzer on rectangular DMA

specimens. 20 x 3 x 1 mm rectangular DMA specimens were machined using a Gravograph 40 W LS100 CO_2 laser machining instrument. DMA experiments were run in the DMA Multi Frequency/Strain mode from 0 to 140°C using a heating rate of 2°C/min, a frequency of 1 Hz, a strain of 0.1%, a preload force of 0.01 N, and a force track of 150%. The data were recorded using TA Instruments Q Series™ software and analyzed using TA Instruments Universal Analysis software. To compare the storage moduli of SMPs containing varying filler compositions, glassy moduli were measured at T_g – 50°C and rubbery moduli were measured at the bottom of the upward sloping modulus curve in each sample's rubbery regime, which occurred at approximately T_g + 40°C.

2.3.2.4 Stress/strain behavior

Strain-to-failure experiments were conducted in accordance with the ASTM D638-Standard Test Method for Tensile Properties on select samples ($n \geq 10$) using an Instron 5965 tensile tester equipped with 1 kN high temperature pneumatic grips, a temperature chamber that utilizes forced convection heating, and a 500 N load cell. The experiments were conducted at T_g – 50°C and T_g + 40°C. ASTM Type V dog bone samples were machined using a Gravograph LS100 40 W CO_2 laser machining device. An Instron Advanced Video Extensometer with a 60 mm field-of-view lens was used to measure sample deformation. For the 110°C tests, the samples were heated to 110°C under zero load (unclamped bottom grip). The samples were then held isothermally for 30 minutes to allow for thermal equilibrium to be reached, after which the bottom grip

was clamped. The experiments were then started using a strain rate of 50 mm/min. Data were recorded using Instron® Bluehill 3 software.

2.3.2.5 Shape memory characterization

Shape memory characterization experiments were performed on rectangular specimens in tension using a TA Instruments Q800 Dynamic Mechanical Analyzer in the DMA Strain Rate mode. The experiments performed were free strain recovery, constrained recovery, and cyclic free strain recovery. 20 x 3 x 1 mm rectangular specimens were machined using a Gravograph 40 W LS100 CO_2 laser cutter. All samples were programmed by heating to 110°C, holding isothermally at 110°C for 20 min, straining the samples to 2.5%, 10%, and 20% deformation, cooling to 20°C, and holding at 20°C isothermally for 20 min. For constrained recovery, the samples were then re-heated to 110°C at 2°C/min without removing the instrument-applied load from the strained samples, and the recovery force of the samples on the instrument was measured. For free strain recovery, the instrument drive force was first set to 0 N before re-heating to 110°C at 2°C/min, and the percent recoverable strain of each sample was measured. For cyclic free strain recovery, the free strain recovery experimental procedures were repeated five times on each sample. The recovery ratio is calculated according to Equation (2),

$$Recovery\ ratio = \frac{Recovery\ length}{Initial\ length} * 100 \quad (17)$$

2.4 Results and discussion

2.4.1 Dispersion

The level of dispersion of the CB and CNT fillers was observed using optical microscopy. Figures 2.1(a) and (e) show that 1% carbon filler compositions CB1 and CNT1 exhibited cluster distribution. With an increase in filler loading to 3%, the CB3 and CNT3 samples begin to exhibit cluster morphology instead of a separated filler composition geometry, as shown in figures 2.1(b) and (f) [58]. In the case of the cluster morphology, carbon fillers connect together to form a network morphology as shown in figures 2.1(c) and (g). Images of the higher density CB7 and CNT7 in the SMP matrix is also shown in figures 2.1(d) and (h). The dispersion percentages of CB and CNT fillers in the SMPs are shown in table 2.1. Complete dispersion is defined by a dispersion value of 100%. The dispersion percentages of CB fillers in the SMP composites are approximately 95 to 98%. For the CNT fillers in the SMP composites, the dispersion percentages are approximately 80 to 84%.

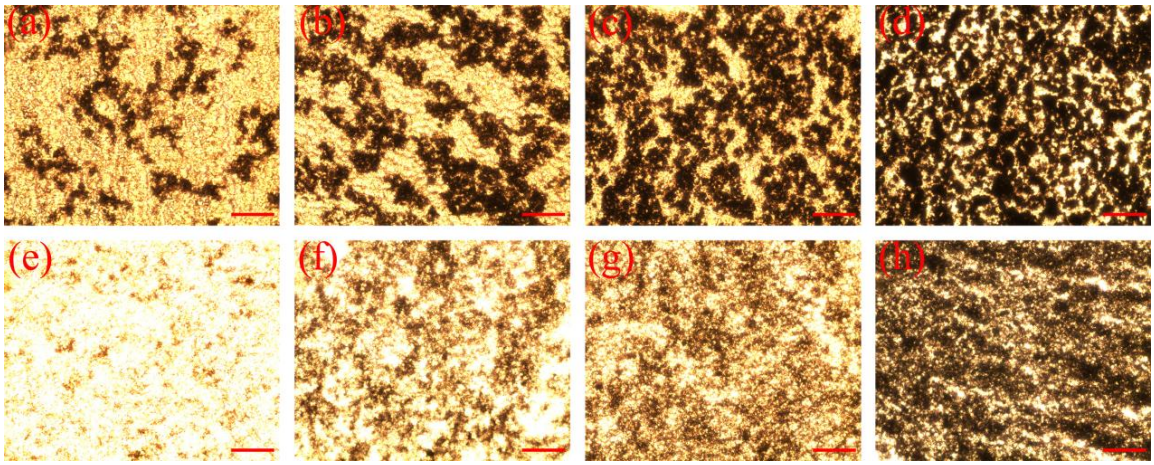

Figure 2.1 Optical microscope images of the distribution of carbon fillers in the SMPs matrix: (a) CB1 is 1 wt% carbon black; (b) CB3 is 3 wt% carbon black; (c) CB5 is 5 wt% carbon black; (d) CB7 is 7 wt% carbon black; (e) CNT1 is 1 wt% carbon nanotube; (f) CNT3 is 3 wt% carbon nanotube; (g) CNT5 is 5 wt% carbon nanotube; (h) CNT7 is 7 wt% carbon nanotube (scale bar, 35μm).

Table 2.1 Percent dispersion of carbon fillers in the SMPs matrix.

Filler loading	Dispersion (%)[a]
CB1	96.3 ± 1.1
CB3	96.5 ± 0.2
CB5	96.7 ± 0.1
CB7	97.3 ± 0.1
CNT1	83.7 ± 6.4
CNT3	82.5 ± 2.3
CNT5	80.2 ± 1.1
CNT7	81.9 ± 0.4

[a]Mean ± stand deviation (n=10)

2.4.2 Glass transition temperature

DSC results, shown in figure 2.2, demonstrate that glass transition temperature decreases slightly from 75 to 71°C with an increase in filler content from 1% to 7%. The

glass transition of a thermoset composite system is dependent on multiple factors, including filler/matrix interactions, filler dispersion, and filler effects on matrix curing (for example, residual moisture in filler particles can alter monomer stoichiometry and in turn influence final network thermomechanical properties) [28]. One possible explanation for the inversely proportional effect of filler composition on glass transition in this study is that filler loading alters the kinetics of the glass transition [29]. With an increase in loaded fillers, the increasing interface area between fillers and matrix may increase polymer chain mobility via plasticization [30].

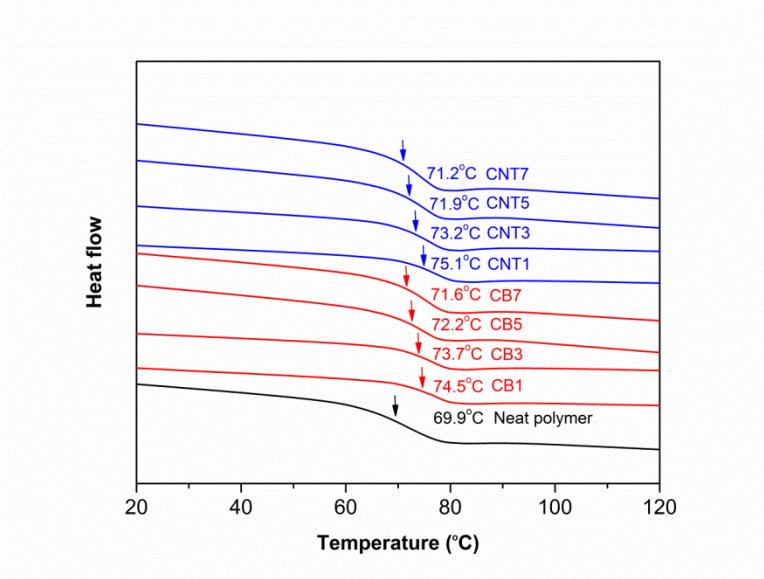

Figure 2.2 DSC results of SMPs composites with various concentrations of CB and CNT fillers.

2.4.3 Storage modulus

Plots of storage modulus versus temperature of the SMP composites with varying filler loading are shown in figure 2.3(a). Plots of storage modulus versus filler composition at 20°C and 110°C are shown in figures 2.3(b) and (c), respectively. The highly crosslinked thermosets in this study undergo roughly a two order of magnitude decrease in storage modulus upon heating through their glass transitions. For example, the storage modulus of the CNT7 sample is roughly 2650 MPa at 20°C while it is in its glassy regime and roughly 37 MPa at 110°C while it is in its rubbery regime. This figure also demonstrates that the increase in added fillers increases the storage modulus of the SMP composites, as predicted. The carbon nanotube fillers increase the storage modulus of the SMPs more significantly than do the carbon black fillers. DMA results, shown in figure 2.3(b), demonstrate that storage moduli at 20°C increase from 2180 to 2520 MPa for carbon black filler loading and from 2300 to 2650 MPa for carbon nanotube filler loading with an increase in filler content from 1% to 7%. Figure 2.3(c) indicates that the rubbery storage modulus at 110°C increases from 21 to 30 MPa with increasing carbon black loading from 1 to 7% and from 25 to 37 MPa with increasing carbon nanotube loading from 1 to 7%.

(a) Loading 7% fillers

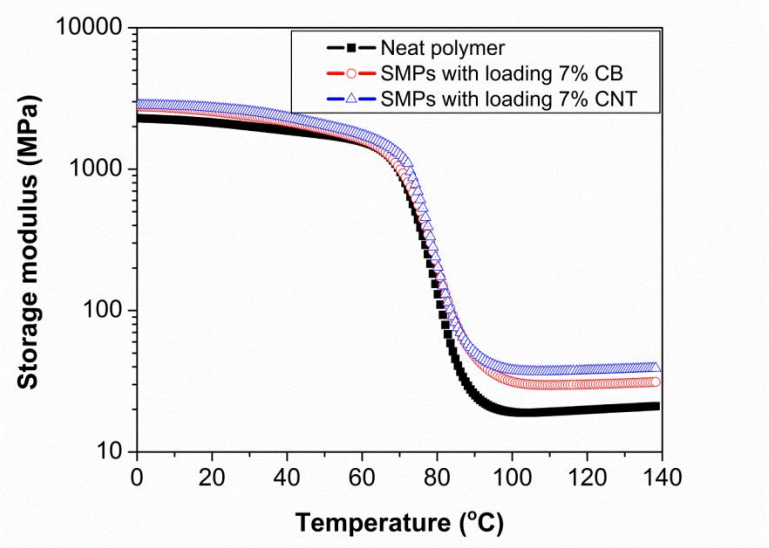

(b) Storage modulus versus the content of carbon fillers at 20°C

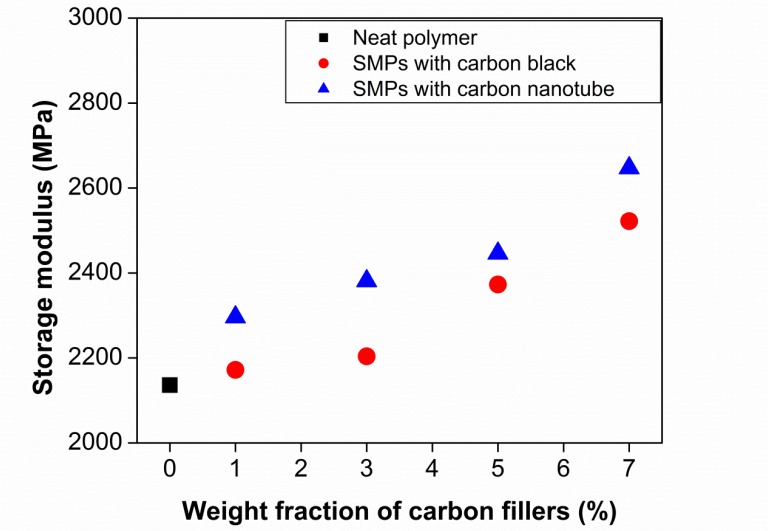

Figure 2.3 Representative storage modulus as a function of temperature for the SMP composites.

(c) Storage modulus versus the content of carbon fillers at 110°C

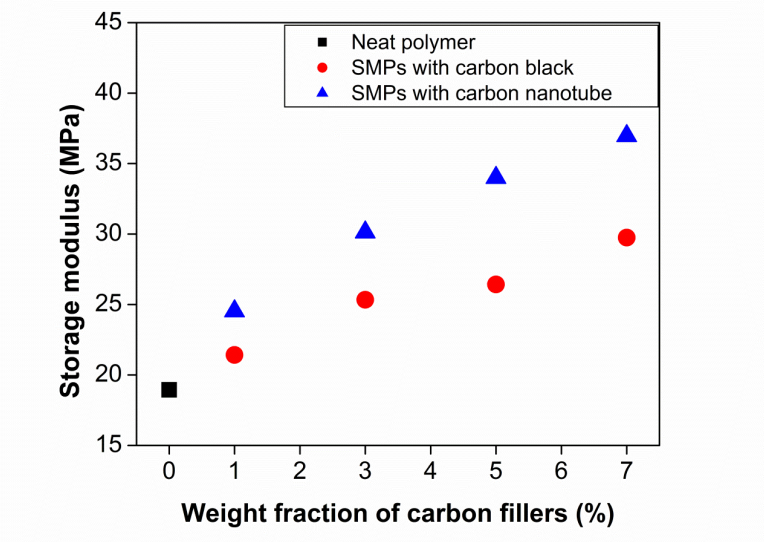

Figure 2.3 Continued.

2.4.4 Stress/strain behavior

Figure 2.4 and Figure 2.5 show typical tensile stress-strain curves of SMP composites with 7% filler loading at 20°C and 110°C, respectively. The stress-strain plots at 20°C resemble those of an amorphous polymer matrix with an initial slope indicative of a high modulus of elasticity and obvious yield behavior [69]. The stress-strain plots at 110°C indicate typical elastomeric behavior, with Young's moduli roughly two orders of magnitude lower than those observed in the glassy regime [59]. The Young's modulus values at 20°C, which were calculated from the slope of stress-strain curves between 0.5 and 1% strain, increase with increasing filler loading as shown in table 2.1. The effect of carbon nanotube filler loading on Young's modulus is more

pronounced than that of carbon black filler loading. This observed trend is expected because, at the structural level, carbon nanotubes are hollow and tubular in structure with walls created by rolled 1-dimensional graphene sheets, which result from covalent bond with sp^2 orbital between carbon atoms, while the carbon black fillers in this study are spherical in nature and comprised of multi-layered graphite to form amorphous structure [31, 70]. Thus, carbon nanotube fillers have a stronger strength than carbon black fillers. In general, increasing filler composition increased ultimate tensile stress and decreased strain capacity at failure. Tables 2.2 and 2.3 show the effects of filler loading on ultimate tensile properties for the polyurethane SMPs for strain-to-failure experiments run at 20°C and 110°C, respectively. Ultimate tensile stress values at 20°C were roughly one order of magnitude greater than those at 110°C, and breaking strains at 20°C were roughly one half of those at 110°C.

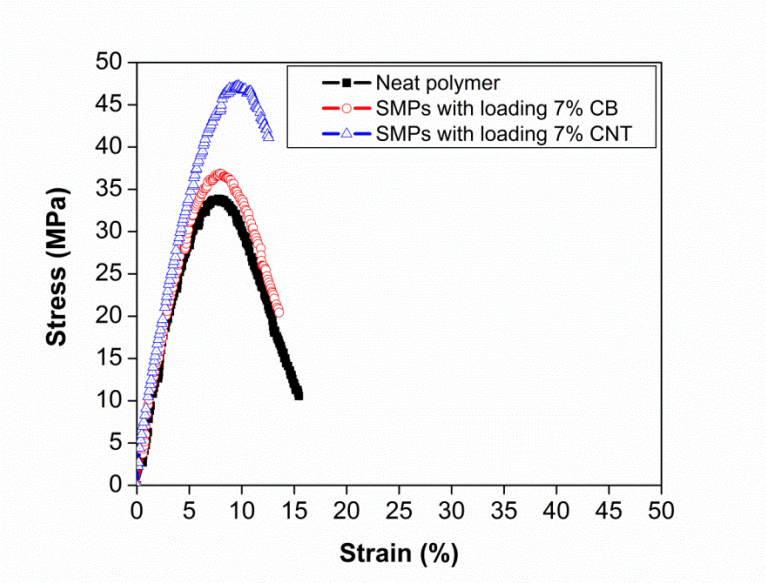

Figure 2.4 Representative tensile stress-strain curve at 20°C for the SMP composites with loading 7% fillers.

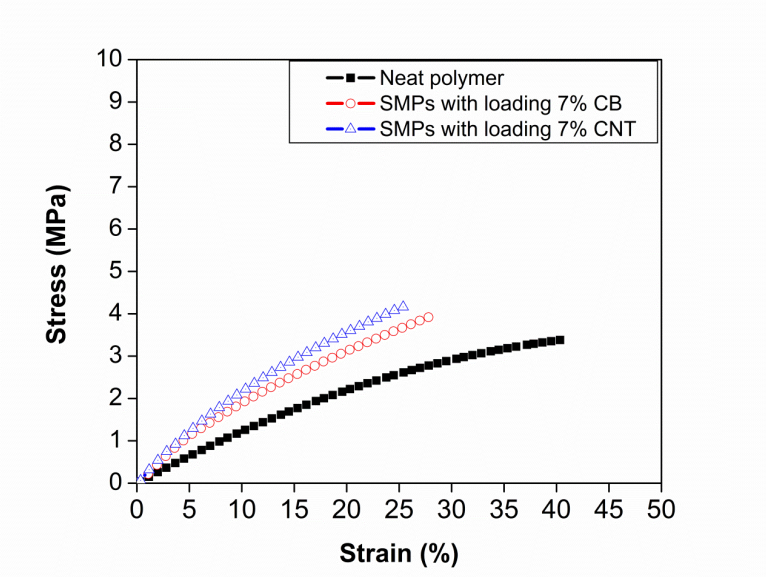

Figure 2.5 Representative tensile stress-strain curve at 110°C for the SMP composites with loading 7% fillers.

Table 2.2 Mechanical properties of SMP composites with different weight fraction of fillers at 20°C.

Filler loading	Ultimate stress (MPa)[a]	Breaking strain (%)[a]	Young Modulus (MPa)[a]
Neat polymer	31.1 ± 2.4	15.3 ± 0.9	2250 ± 170
CB1	33.7 ± 1.1	14.5 ± 0.8	2410 ± 280
CB3	34.5 ± 2.1	13.1 ± 1.7	2720 ± 130
CB5	35.9 ± 5.0	12.9 ± 0.7	2930 ± 160
CB7	36.8 ± 4.7	12.8 ± 0.8	3120 ± 220
CNT1	34.7 ± 4.7	12.8 ± 3.7	2690 ± 120
CNT3	38.1 ± 6.3	12.4 ± 2.9	3050 ± 230
CNT5	41.1 ± 5.7	12.0 ± 2.4	3440 ± 210
CNT7	43.9 ± 5.2	11.4 ± 1.6	3890 ± 310

[a]Mean ± stand deviation (n=10)

Table 2.3 Mechanical properties of SMP composites with different weight fraction of fillers at 110°C.

Filler loading	Ultimate stress (MPa)[a]	Breaking strain (%)[a]	Young Modulus (MPa)[a]
Neat polymer	3.0 ± 0.4	40.4 ± 0.3	20.9 ± 0.7
CB1	3.1 ± 0.4	30.1 ± 6.9	21.6 ± 0.6
CB3	3.5 ± 0.3	27.3 ± 1.1	23.6 ± 0.9
CB5	3.6 ± 0.7	27.0 ± 2.3	26.4 ± 2.5
CB7	3.9 ± 0.1	26.4 ± 2.6	27.7 ± 0.7
CNT1	3.2 ± 0.8	30.6 ± 7.6	22.7 ± 0.5
CNT3	3.5 ± 0.6	29.2 ± 6.3	26.8 ± 1.7
CNT5	3.9 ± 0.9	26.4 ± 6.4	29.5 ± 1.6
CNT7	4.4 ± 0.9	22.5 ± 5.9	35.8 ± 2.3

[a]Mean ± stand deviation (n=10)

2.4.5 Shape memory property

Shape memory properties, namely free strain recovery, stress recovery under

constrained strain, and cyclic free strain recovery of the SMP composites are discussed in this section. Table 2.4 contains single-cycle free strain recovery data for the SMP composites strained to 2.5%, 10%, and 20% deformations. As filler loading increases from 0 to 7%, first-cycle recoverable strain decreases, and the extent of irrecoverable strain increases with increasing deformation level. A more significant decrease in recoverable strain is observed for CNT filler loading than for CB filler loading. With 2.5% pre-strain extension, the recovery ratio of all CB-filled samples and 0, 1, and 3% CNT-filled samples approaches 100%, and for 5 and 7% CNT-filled samples, the recovery ratio decreases to roughly 95%. With 10% pre-strain, the CB-filled composites still exhibit roughly 85% recovery, while the CNT-filled composites exhibit 70-75% recovery. For 20% pre-strain, the observed recovery ratio is in the range of 60-70%.

Table 2.5 contains recovery stress data for the SMP composites obtained using constrained recovery analysis. Previous studies have shown that recovery stress is dependent on numerous factors, including pre-strain extension, crosslink density, and filler type and composition [7]. In this study, increasing both pre-strain extension and filler composition resulted in increased recovery stress. These trends are consistent with those reported by Gunes *et al* [7], who have previously demonstrated that both increased pre-strain extension and increased filler loading (organoclay, carbon black, carbon nanofiber, and silicon carbide) result in increased recovery stress of SMP composite systems. Also, the CNT filler is observed to increase recovery stress in a more pronounced manner than the CB filler. Previous studies, such as those reported by Rousseau *et al* [18], summarized that recovery stress of composite SMPs increases with

increasing rubbery modulus, and that fillers resulting in the greatest rubbery modulus increases also result in the greatest recovery stress increases. figure 2.3(c) demonstrates that, for the SMP composites in this study, CNT loading results in a greater rubbery modulus increase than does CB loading.

Figures 2.6(a) and 2.6(b) contain 5-cycle cyclic free strain recovery data for 10% pre-strain extension for CB and CNT-filled samples, respectively. After the second cycle of free strain recovery, the CB7 composite sample exhibits a 100% recovery ratio, while the CNT7 composite sample only exhibits an 88% recovery ratio and did not exhibit a 100% recovery ratio until cycle 4 (table 2.6). As shown in figure 2.3(a), the glassy storage modulus of the CNT7 composite is greater than that of the CB7 composite. Previous studies have shown that the recoverable strains of SMP composites decrease with increased filler loading [71]. Gall *et al* [71] have demonstrated that loading filler particles stores internal elastic strain energy during pre-strain extension and that the stored elastic strain energy in the fillers can be released during cyclic free strain recovery. After several cyclic strain recovery cycles, the recovery ratio of the SMP composites approaches 100% [72].

Table 2.4 Strain recovery ratio of SMP composites.

Filler loading	Recovery ratio (%)		
	2.5% strain	10% strain	20% strain
Neat polymer	100	100	100
CB1	100	82	68
CB3	98	84	73
CB5	100	84	70
CB7	99	88	69
CNT1	99	71	69
CNT3	100	70	61
CNT5	95	77	66
CNT7	94	68	63

Table 2.5 Recovery stress of SMP composites.

Filler loading	Stress recovery (MPa)		
	2.5% strain	10% strain	20% strain
Neat polymer	0.19	1.02	1.62
CB1	0.41	1.19	2.15
CB3	0.43	1.31	2.69
CB5	0.48	1.33	2.72
CB7	0.54	1.67	2.83
CNT1	0.49	1.37	2.31
CNT3	0.49	1.58	2.35
CNT5	0.58	1.66	2.71
CNT7	0.61	1.81	3.01

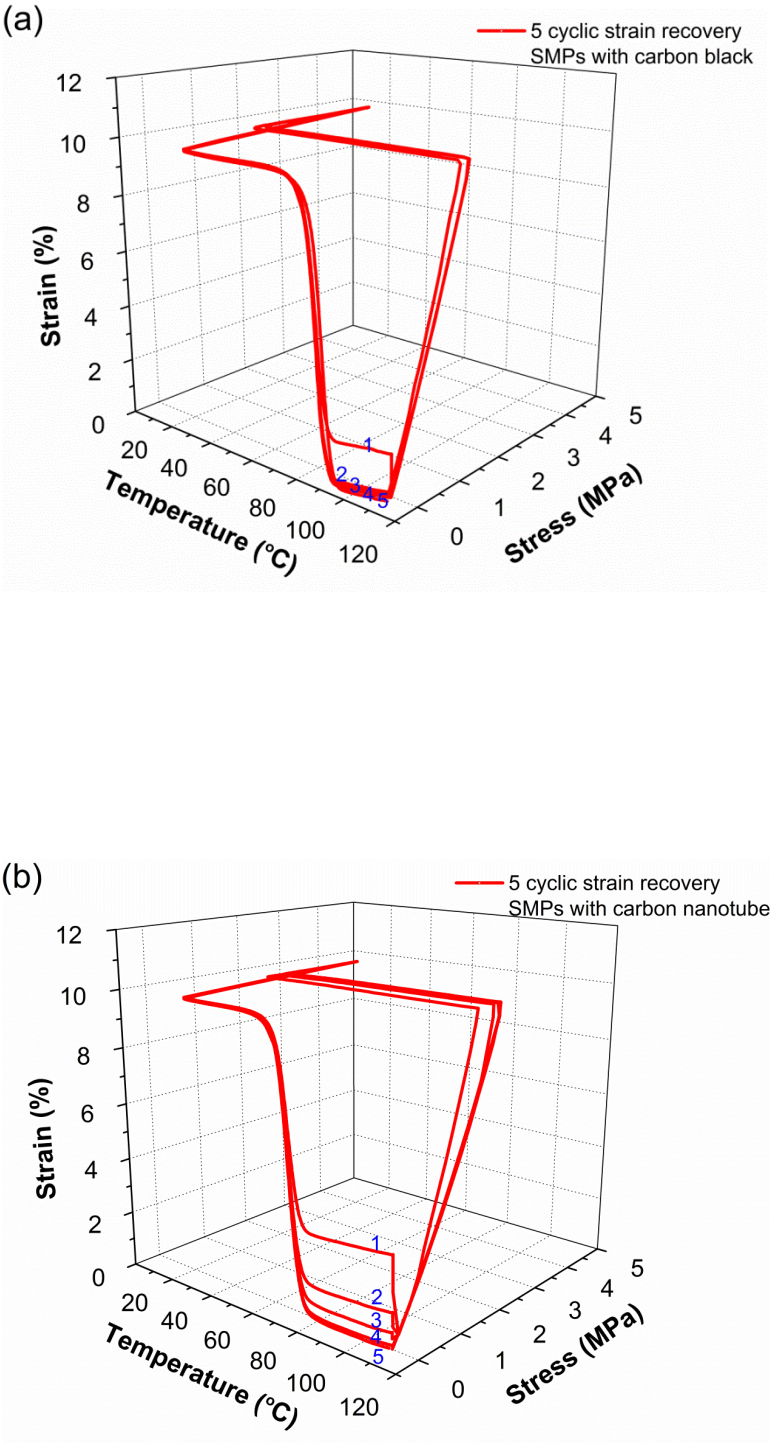

Figure 2.6 Plot of cyclic strain recovery evaluated by SMP composites (a) CB7; (b) CNT7.

Table 2.6 Cyclic strain recovery of SMP composites.

Cycle	Recovery ratio (%)				
	1	2	3	4	5
Neat polymer	99	100	100	100	100
CB7	87	100	100	99	100
CNT7	69	88	94	99	100

2.5 Conclusions

The effects of carbon black and carbon nanotube filler loading on the thermal, thermomechanical, and shape memory properties of a highly crosslinked, aliphatic thermoset polyurethane shape memory polymer composite system are reported in this study. As filler loading increased from 0 to 7%, the glass transition temperature of the SMP composites decreased slightly, from 75 to 71°C. Increasing filler composition also resulted in increased glassy and rubbery moduli and increased recovery stress; however, this increase in modulus and recovery stress was accompanied by a decrease in recoverable strain capacity. In general, carbon nanotube loading resulted in both a higher modulus and recovery stress increase and a more significant decrease in recoverable strain capacity than did carbon black loading.

Only limited studies have been conducted on thermoset SMP composite systems. Studies that have been conducted on thermoset composites have been focused on three main systems: styrene, epoxy, and acrylate-based systems. This paper reports the synthesis and thermomechanical characterization of a new urethane-based thermoset SMP composite system. Loading of carbon fillers into our SMP system could not only

improve mechanical properties, but could also enable shape recovery actuation of pre-strained secondary geometries by resistive heating by exploiting the polymer filler's thermal conductivity properties. In Part II, we will examine the effect of varying quantities of carbon fillers in the SMP matrices on electrical resistivity to determine the percolation threshold.

CHAPTER III

CARBON FILLERS FOR ACTUATION OF ELECTROACTIVE THERMOSET SHAPE MEMORY POLYURETHANE COMPOSITES BY RESISTIVE HEATING – PART II

3.1 Overview

This study focuses on electroactive thermoset shape memory polyurethane composites containing carbon black and carbon nanotube at various loading levels. In Part I we focused on the thermomechanical behavior of thermoset urethane-based shape memory polymer (SMP) composites with carbon filler. In Part II, by increasing the filler content to over the percolation threshold, the electrical resistivity of SMP composites is lowered to 10^3 Ω cm with carbon black filler and 10^2 Ω cm with carbon nanotube filler. Due to the increase in electrical resistivity caused by positive temperature coefficient effect and changes in electrical resistance induced by strain extension, stable heat conductivity is provided by loading 5wt% carbon black and 4.5wt% carbon nanotube. Also, with the maximum loading of 7wt% for both carbon black and carbon nanotube, the shape memory recovery of these electroactive composites is the function of time by applying different voltage.

3.2 Introduction

Shape memory polymers (SMPs) can be deformed from their original shape to a temporary shape after heating to above their transition temperature, and they can remain

in the temporary shape by subsequently cooling below their transition temperature while maintaining the deformation. The temporary shape of SMPs can recover back to their original shape under appropriate external stimulus [3, 56, 72], including heat [16], light [11], electrical field [12], magnetic field [13], and moisture [14, 73]. Traditionally, most researchers have used direct heat to actuate the deformed SMPs. However, the traditional direct heating limits the potential applications of the SMP device [18]. To increase the heat conductivity, past studies have blended the polymer with conductive fillers such as nickel particles [5], carbon fibers [57], carbon nanotube [26], and carbon black [58].

The conductivity of the polymer is directly related to the amount of conductive fillers added to the polymer matrix. When the fraction of fillers in the matrix is very low, the mean distance between fillers is too far for electrical conductivity, and the insulating polymer matrix limits the material's conductivity. On the other hand, when the filler is above the critical concentration, the filler distribution becomes close enough to generate a conducting path so that an electron can pass through the disordered network of fillers. This critical concentration of filler is called the percolation threshold [32]. Recently, various conductive fillers have been added into thermoplastic urethane-based SMP composites to derive multiple applications. Cho *et al* [25] investigated the urethane-based SMPs with modified multiwall carbon nanotube (CNT) by solution mixing and sonication. With loading 5 wt% modified MWCNT, the electrical resistivity (ρ) was lowered to 10^3 Ω cm, and they then demonstrated the potential for SMP to actuate by Joule heating. Gunes *et al* [6] studied the electroactive urethane-based SMPs with added

carbon nanofiber (CNF), oxidized carbon nanofiber (ox-CNF), and carbon black (CB) in mixer. The percolation threshold of theses system occurred at loading around 4 wt% CNF, 5 wt% ox-CNF, and 4 wt% CB with $\rho \sim 10^5$ Ω cm. Only the SMP composites with CB showed a significant positive temperature coefficient (PTC), which means the electrical resistivity increases with increasing temperature. The PTC resulted in a thermal expansion of matrix larger than that of CB, and its resistivity increased several orders of magnitude with imposed strain extension. Li *et al* [9] investigated the urethane-based SMP with loading 30 wt% CB to achieve the percolation threshold ($\rho \sim 10$ Ω cm). With an increase in CB loading, the ratio of shape memory recovery significantly decreases.

Compared to thermoplastic SMP, thermoset SMP sometimes shows advantages in the cyclic shape memory behavior as well as higher recovery stresses [61]. However, only limited studies have been conducted on the thermoset SMP composites system because of process limitations in synthesis and mixing technologies [18, 58]. For example, in the process of urethane-based thermoset polymer, isocyanates react with water to generate carbon dioxide bubbles, which exist in the matrix. Therefore, thermoset polymers cannot be melted and reset without destroying the internal crosslinking network of the urethane-based matrix to evaporate the bubbles. Previous efforts on thermoset SMP composites have been focused on three systems: (1) Stryene-based system: Leng *et al* [5, 57, 58, 74] added different carbon fillers into this system to study their electrical properties of SMP composites; (2) Epoxy-based system: Gall *et al* [71] and Liu *et al* [59] loaded SiC into epoxy-based SMP to reinforce the matrix and

measure their thermomechanical behavior; (3) Acrylate-based system: Schmidt *et al* [75] and Yakacki *et al* [60, 75] incorporated Fe_3O_4, or magnetite, into acrylate-based SMP to remotely heat the SMP composites via exposure to a magnetic field.

In this work, the use of thermoset urethane-based SMPs based on materials developed by Wilson *et al* [61] is investigated, with the matrix material containing CB and CNT fillers. This study is focused on finding the percolation threshold of thermoset urethane-based SMP composites with CB and CNT to be measured by four point probe. Also, to achieve the minimum amount of filler loading, this value is determined by the ratio of resistance of SMP composites with different strain extension and by the plot of temperature dependent electrical resistivity of SMP composites. The shape memory recovery rate and the ratio of deformed electroactive SMP composites were measured by applying voltage.

3.3 Experimental

The urethane-based thermoset SMP composites were prepared from the trifunctional polyol triethanolamine (TEA; Sigma Aldrich, 99%), the tetrafunctional polyol *N,N,N',N'*-tetrakis(2-hydroxypropyl) ethylenediamine (HPED; TCI America, 98%), and hexamethylene diisocyanate (HDI; TCI America, 98%). The carbon fillers used were carbon black (CB; Ensaco 250, primary particle size ~40 nm, density 0.17 g cm^{-3}), and multi-wall carbon nanotubes (CNT; Sigma Aldrich 659258, purity 90%, dimensions 110-170 nm x 5-9 μm (diameter * length), density 1.7 g cm^{-3}, surface area 1.3 x 10^2 m^2 g^{-1}). The CB and CNT were dispersed in the viscous monomer HPED in 1,

3, 5, and 7 wt% ratios by using a FlackTek™ SpeedMixer™ DAC 150 speed mixer at 3400 rpm with dispersion times of 0.5, 1, 1.5, and 2 min. TEA and HDI were subsequently added to the mixture using the same speed mixer settings. The SMP composites were cured at room temperature for 2 h and then heat treated to polymerize at 120°C for 1 h. Finally, the SMP composites were polished by computer numerical control (Roland MDX-540) into 1~2 mm in thickness.

3.3.1 Electrical resistivity

In order to determine the resistivity of SMP composites with carbon fillers, 30 x 5 x 2 mm rectangular specimens were machined using Gravograph 40 W LS100 CO_2 laser machining instrument. The resistivities were measured with an in-house four-point probe SP4 (Signatone) apparatus with Agilent 34401A multimeter, Agilent 34420A micro-ohm meter, and Agilent E3632A DC power supply.

3.3.2 Positive temperature coefficient effect

To evaluate the effect of temperature on the resistivity of SMP composites with carbon fillers (CB is 4wt%, 4.5wt% and 5wt%; CNT is 3.5wt%, 4wt% and 4.5wt%), 10 x 10 x 1 mm rectangular specimens were characterized using resistivity-temperature (R-T) measurement from 25 °C to 105 °C with heating rate 1 °C/min in a physical property measurement system (PPMS, Quantum Design).

3.3.2.1 Thermal expansion

Thermomechanical analysis tests were performed on a TA Instruments Q400 machine to obtain the coefficients of thermal expansion (CTE) for the neat polymer above and below the glass transition temperature. A cylindrical specimen approximately 4mm in diameter and 6mm in length was subjected to one cycle in which the temperature was raised from 0 °C to 120 °C at a heating rate of 1 °C/min.

3.3.3 Changes in electrical resistance induced by strain extension

The resistances of SMP composites (CB is 4wt%, 4.5wt% and 5wt%; CNT is 3.5wt%, 4wt% and 4.5wt%) were measured with different strain extensions 2.5%, 5%, 10%, 15%, and 20% , which were below the breaking strain of approximately 25% to 30%. All samples were programmed by heating to 110°C, holding isothermally at 110°C for 20 min, straining the samples to the above different strain extensions, and cooling to 20°C for 20 min. The test method followed the same setting of section 3.3.1.

3.3.4 Electroactive shape memory effect

The specimens of SMP composites with 7wt% CB and CNT were bent 180 degrees into their temporary shapes. The specimens were actuated by different constant voltages (Agilent 6209B DC power Supply) through two conductive clamps and were recorded by video (Panasonic HDC-HS80).

3.4 Results and discussion

3.4.1. Electrical resistivity

The electrical resistivity as function of conductive filler weight fraction of the SMP composites is shown in figure 3.1. The SMP composites with carbon black reached the percolation threshold at a filler concentration of around 3wt% to 4wt%, and the electrical resistivity (ρ) was lowered to 10^3 Ω cm, which is similar to previous results in the literature [5, 6, 42, 57, 58]. The electrical percolation for the composites with carbon nanotubes is around 2.5wt% to 3.5wt%, and electrical resistivity is lowered to 10^2 Ω cm. The lowered electrical resistivity means that a new network formation of conductive fillers was formed in the matrix. Also, the plot of both loading fillers CB and CNT indicated that a further increase in filler loading over the percolation threshold shows no significant decrease in electrical resistivity [32].

To demonstrate the result of approaching the filler concentration of percolation threshold, two different shapes of sphere and stick of percolation theory were used. Following the equation of the percolation threshold of sphere shape derived by Liang *et al* [42], SMP composites with CB were around 4.5wt%. Also, following the equation of the percolation threshold of high-aspect-ratio stick shape derived by Berhan *et al* [43], the percolation threshold of SMP composites with CNT is around 1.1 to 3.4wt% because of a range of different aspect ratios of CNT. The theory of percolation threshold of SMP with loading CB indicated that the connective network is generated in the matrix before achieving the ideal value. However, with loading carbon nanotube, the result is a little higher than the theory value. Our studies in Part I indicated that the dispersion of CB

fillers is approximately 96 to 98% and the dispersion of CNT fillers is approximately 80 to 84% in the SMP composites matrix. Complete dispersion is defined as a dispersion value of 100%. Due to strong Van der Waals energy interactions, CNT tend to aggregate, resulting in limited uniform dispersion when compared to CB [45].

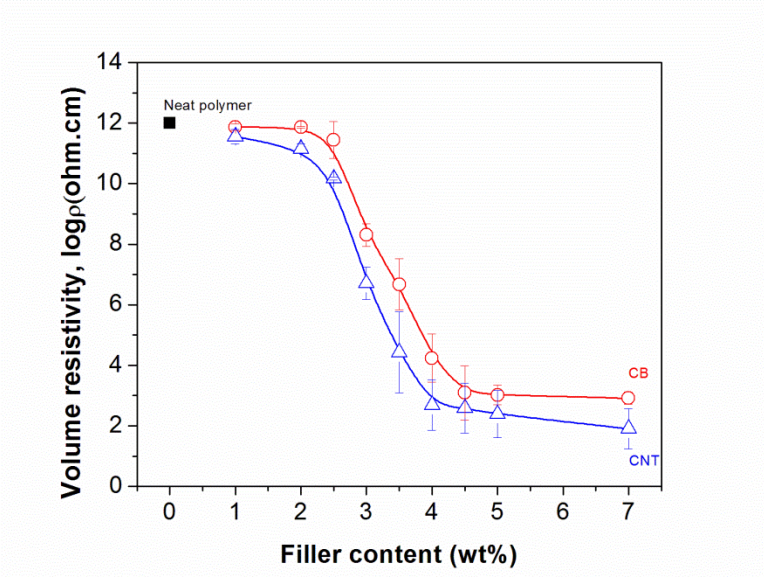

Figure 3.1 Electrical resistivity of the SMP composites filled with CB and CNT.

3.4.2 Positive temperature coefficient effect

The dependence of the electrical resistivity on temperature of the SMP composites is shown in figure 3.2. The electrical resistivity of CB4 increased by 3 orders of magnitude as the temperature was increased from 75 to 105°C. On the other hand, CB4.5 increased by 1 order of magnitude after temperature was raised higher than 75°C.

However, the plot of electrical resistivity of CB5 shows no significant change. Generally, the electrical resistivity of a conductive polymer gradually increases with an increase in temperature. This phenomenon is called positive temperature coefficient (PTC). The PTC effect is used to explain the breakdown of the continuous conductive network because of the different thermal expansion of polymer matrix compared to its fillers. With an increase in temperature, the gap between conductive fillers increases so that the electrons cannot travel between them [32]. With an increase in CB loading, the electrical resistivity becomes relatively stable with an increase in temperature because the higher CB loading in the SMP matrix maintains a more continuous conductive network when heated when compared to lower CB loading [58]. Also, figure 3.2 indicates that CNT3.5 and CNT4 increased only slightly after temperature was raised higher than 75°C. Therefore, the plot of electrical resistivity of CNT4.5 shows no significant change. In this study, when compared to CB, no obvious change of the electrical resistivity of SMP composites was observed with loading CNT. Due to the high aspect ratio of CNT, the fillers present a more stable and conductive interconnect network in the SMP matrix [6].

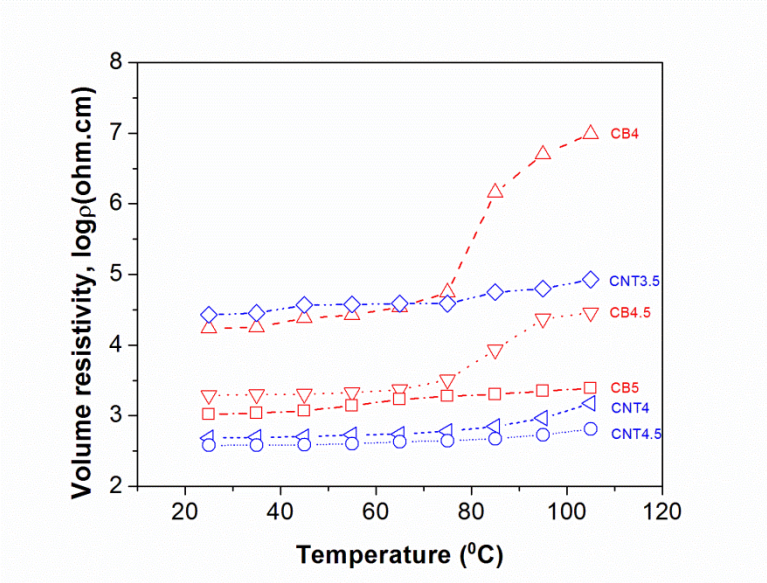

Figure 3.2 Temperature dependent electrical resistivity of SMP composites.

3.4.2.1 Thermal expansion

The coefficients of thermal expansion (CTE) in the glassy and rubbery phases were calculated as the slopes of the linear dimension change vs. temperature data from 20°C to 50°C and 85°C to 105°C, respectively, as shown in figure 3.3. The resulting CTE for the glassy and rubbery phases are 7.9 x 10^{-5}/°C and 2.1 x 10^{-4}/°C. The increase in temperature over T_g enables long-range movement of the polymer chains, which results in a higher CTE. The CTE of carbon black similar to the CTE of graphite 4.1 x 10^{-6}/°C was used [77]. Also, the CTE of multiwall CNT is negative because of structural and vibrational entropy resulting in a decrease in size [78, 79]. In figure 3.3, the plot of CTE of neat polymer indirectly validates the trend of temperature dependent electrical resistivity of SMP composites (figure 3.2), especially for SMP composites with loading

a lower amount of fillers of CB. This means that with an increase in temperature, the material matrix has a larger thermal expansion than that of its fillers, resulting in an increase in distance between the fillers, making conduction more difficult [58]. Therefore, the system of SMP composites with loading CNT shows the relatively stable plot when compared to the system with loading CB [6]. Even the temperature causes the increase in CTE of neat polymer to increase the matrix's dimension; the high aspect ratio of CNT fillers provides the stable conductive network in the matrix.

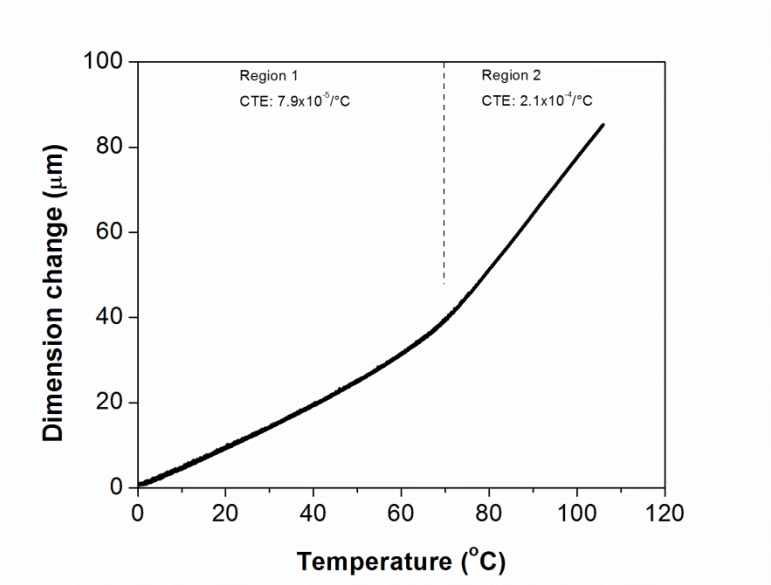

Figure 3.3 Thermal expansion behavior of neat polymer.

3.4.3 Changes in electrical resistance induced by strain extension

Stable electrical conductivity is achieved when the resistive heating for actuating the temporary shape of SMP composites is constant. With different amounts of fillers of SMP composites, the ratio of changes in electrical resistance induced by strain extension is the resistance of stretched specimen (R) in the axial direction to the original resistance (R_0). In figure 3.4, the plot of R/R_0 of SMP composites with loading 4.5wt% and 4wt% carbon black showed an increasing trend. However, the resistance of SMP composites with loading 5% carbon black with longer strain extension showed a plateau in the plot. Also, the SMP composites with carbon nanotubes showed a similar trend but with a smaller increase in R/R_0. The resistance of the 3.5wt% and 4wt% CNT systems increased with an increase in strain extension. However, the system with loading 4.5wt% CNT increased only slightly with strain up to 5wt% and then again performed a plateau in tensile strain. Due to the high aspect ratio of CNT, the filler possibly maintains stable conductivity so as to preserve the conductive network in the matrix with a high strain extension [6]. Also, with an increase in the amount of fillers, the plot of R/R_0 of SMP composites tended to show a stable plateau with larger strain extension [80]. In past studies, the elongation increased the gap between fillers in the matrix, resulting in breaking the original conductive network. However, for stick shape fillers, the elongation enhanced the CNT fillers in the matrix by causing reorientation along the direction of stretch to generate a new conductive network [81]. For sphere shape fillers, with an increase in CB fillers loading, there is less of an effect of network-breakdown

phenomena [6]. Finally, for stable heat conductivity, the minimum filler loading in the SMP composites is 5wt% for CB and 4.5wt% for CNT.

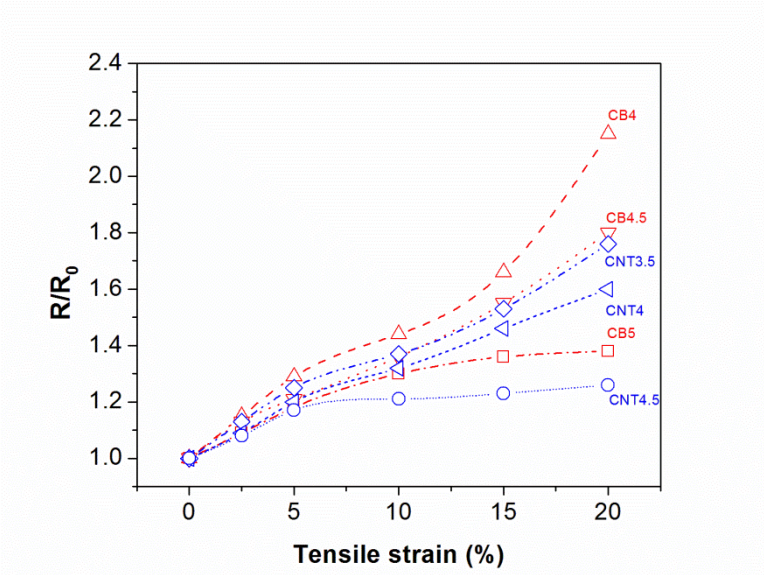

Figure 3.4 The ratio of resistance of SMP composites with different strain extension.

3.4.4 Electroactive shape memory effect

Resistive heating was used to actuate a sample of CNT7 from its temporary shape in figure 3.5. The sample dimension of SMP composites CB7 and CNT7 are machined into a dimension as shown in the left inset of figure 3.5. The samples CB7 and CNT7, bent 180 degrees into their temporary shape, were actuated by different constant voltages through two conductive clamps (figure 3.6). In figure 3.6(a), the temporary shape of sample CB7 is actuated by 200 V and 240 V to recover around 150 to 160

degrees from its deformed shape. However, the recovery after applying 160 V on sample CB7 was 45 degrees, and applying 120 V yielded no significant response. In figure 3.6(b), 120 V, 160 V, and 200 V were applied on samples of CNT7, and the recovery was similar to CB7 at around 150 to 160 degrees. However, the recovery rate when applying 120 V was slower than the two others and needed around 450 seconds to achieve its final recovery angle. The recovery ratios of composite samples of CB7 and CNT7 were about 83%-88% when compared to their original shapes. Also, the recovery rate of sample CNT7 was faster than the samples of CB7. For example, under the same applied voltage of 200 V, the recovery rate of CB7 samples spent 90 seconds achieving their final recovered shape; however, samples CNT7 only needed 30 seconds for final recovery.

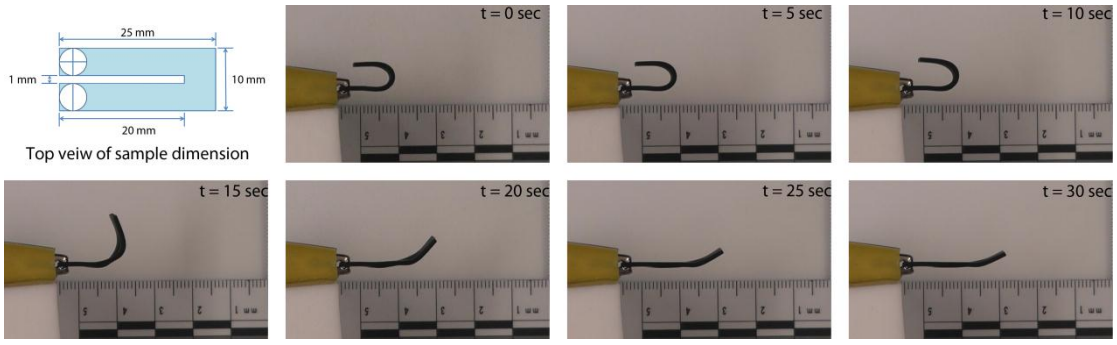

Figure 3.5 Sequences of the electroactive shape memory recovery of sample CNT7 by applying 200 volts.

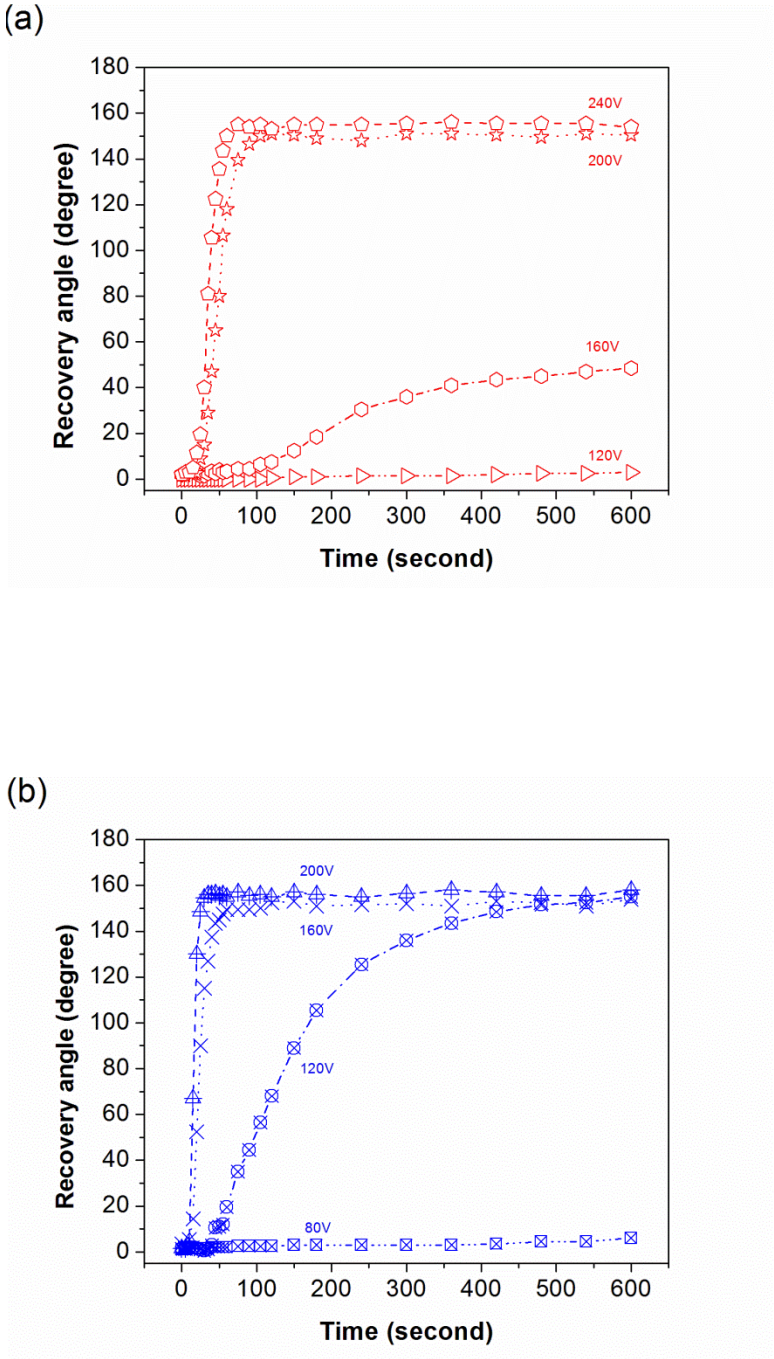

Figure 3.6 Recovery angle of sample as function of time by applying different voltage. (a) CB7; (b) CNT7.

3.5 Conclusions

The networks of carbon fillers facilitate the resistive heating to allow for actuation of SMP composites through an applied voltage. The filler network significantly increases the electrical conductance of the material matrix when compared to the non-doped polymer. The percolation threshold of thermoset urethane-based SMP composites is 3wt%-4wt% with loading CB fillers and is 2.5wt%-3.5wt% with loading CNT fillers. This concentration allows the fillers to be close enough in proximity to generate a conducting path for electricity. For stable heat conductivity, both results show the PTC effect caused the increase in electrical resistivity and electrical resistance induced by strain extension up to 20%, indicating that samples with loading 5wt% CB fillers and 4.5wt% CNT fillers facilitate an electron passing through the continuous conductive network. Both of the recovery ratios of SMP composites with CB7 and CNT7 are around 83%-88%.

CHAPTER IV

SILICONE MEMBRANES TO INHIBIT WATER UPTAKE INTO THERMOSET POLYURETHANE SHAPE-MEMORY POLYMER CONDUCTIVE COMPOSITES

4.1 Overview

Electroactive shape memory polymer (SMP) composites capable of shape actuation via resistive heating are of interest for various biomedical applications. However, water uptake into SMPs will produce a depression of the glass transition temperature (T_g) resulting in shape recovery *in vivo*. While water actutable shape recovery may be useful, it is foreseen to be undesirable during early periods of surgical placement into the body. Silicone membranes have been previously reported to prevent release of conductive filler from an electroactive polymer composite *in vivo*. In this study, a silicone membrane was used to inhibit water uptake into a thermoset SMP composite containing conductive filler. Thermoset polyurethane (PU) SMPs were loaded with either 5wt% carbon black (CB) or 5wt% carbon nanotubes (CNT) and subsequently coated with either an Al_2O_3- or silica-filled silicone membrane. It was observed that the silicone membranes, particularly the silica-filled membrane, reduced the rate of water absorption (37°C) and subsequent T_g depression versus uncoated composites. In turn, this led to a reduction in the rate of recovery of the permanent shape when exposed to water (37°C).

4.2 Introduction

Thermosensitive shape memory polymers (SMPs) are one type of smart materials [3]. The permanent geometry can be sequentially deformed into a temporary geometry when heated above the transition temperature (T_{trans}), the secondary geometry fixed by cooling below T_{trans} and the original shape recovered upon heating above T_{trans}. Conductive fillers such as carbon carbon black (CB) [82], nanotubes (CNT) [26], and carbon nanofibers [6] have been incorporated into thermoplastic SMP systems to actuate the shape recovery via voltage-induced current rather than environmental heat.

The addition of fillers into the SMP matrix can increase the recovery stress as well as improve other mechanical properties such as modulus [7]. While thermoset SMP systems have the potential to achieve robust mechanical properties, few studies have been focused on these because of synthetic and processing limitations [18, 63]. As a result, thermoset SMP composites have been largely limited to styrene-based systems with conductive carbon filler [5], epoxy-based systems reinforced with SiC [59], and acrylate-based systems with magnetic Fe_3O_4 particles [60].

Polyurethane (PU) SMPs have drawn significant attention for a broad range of applications [15, 83]. While the vast majority are thermoplastics, thermoset PU SMP systems having high recovery strains and stresses have been reported with potential use for biomedical applications [61]. In addition, we have reported ultra-low destiny thermoset PU SMP foams that undergo high volumes changes upon recovery from compressive strain and thus may have utility as embolic sponges to treat aneurysms [84, 85].

The effect of water uptake on shape memory behavior and physical properties of thermoplastic PU SMPs has been reported [14]. It was shown that moisture absorption led to a decrease in T_g due to weakening of the hydrogen bonding between N-H and C=O groups. Thus, the absorbed water acted as a plasticizer [86]. Due to the decreased T_g (i.e. decreased T_{trans}), a loss of shape fixity was also observed and specimens exhibited shape recovery upon immersion in 37°C water. In the case of conductive SMP composites, release of conductive fillers *in vivo* remains yet another substantial concern [87]. For this reason, various membranes such as parylene C [88, 89], polytetrafluoro ethylene [90], and silicones [91, 92] have been proposed as protective barrier coatings. Thus, the utility of thermoset PU SMP conductive composites in biomedical applications would be enhanced if the water absorption and potential release of filler could be controlled. However, the use of such a membrane to impede water absorption into an SMP conductive composite has not yet been explored.

Herein, thermoset PU SMP conductive composites were prepared with CB and CNT fillers and coated with a silicone membrane to hinder water absorption. In terms of biomedical applications, the extreme hydrophobicity [93, 94], as well as biocompatibility, biodurability, and thermal and oxidative stability [53, 95, 96] makes silicones an ideal candidate. Since silicones are typically reinforced [96], both an Al_2O_3- and silica-filled silicones were evaluated in this study. The silicone-coated SMP composites were subjected to conditioning in water (37°C) and the resulting water uptake as well as rate and extent of the T_g depression were compared to uncoated

controls. In addition, shape recovery (i.e. diminished shape fixity) of coated- and uncoated-SMPs in a 37°C aqueous environment was compared.

4.3 Experimental

4.3.1 Materials

Trifunctional polyol triethanolamine (TEA; Sigma Aldrich, 99%), tetrafunctional polyol *N,N,N',N'*-tetrakis (2-hydroxypropyl) ethylenediamine (HPED; TCI America, 98%), and hexamethylene diisocyanate (HDI; TCI America, 98%) were used as received. CB (ENASCO® 250; primary particle size ~40 nm, density 0.17 g cm^{-3} per manufacturer's specification) was obtained from TIMCAL Graphite & Carbon. Multiwall CNTs (dimensions 110-170 nm x 5-9 μm, density 1.7 g cm^{-3} per manufacturer's specification) were obtained from Sigma Aldrich. Al_2O_3-filled silicone (SYLGARD® Q3-3600) was obtained from Dow Corning. Per manufacturer's specifications, Q3-3600 is comprised of: *Part A*: methyltrimethoxysilane treated aluminum oxide (70-90%), dimethyl siloxane (15-35%), methylvinyl siloxane (1-5%), and methyl alcohol (<0.01%); *Part B*: methyltrimethoxysilane treated aluminum oxide (70-90%), dimethyl siloxane (15-35%), methylhydrogen siloxane (3-7%), carbon black (<1%), and methyl alcohol (<0.01%). Medical-grade silica-filled silicone (MED-1137) was obtained from NuSil Technology. Per manufacturer's specifications, MED-1137 is comprised of: α,ω-bis(Si-OH)PDMS, silica (11-21%), methyltriacetoxysilane (<5%), ethyltriacetoxysilane (<5%), and trace amounts of acetic acid. Hexane (95%,

anhydrous) was obtained from Sigma Aldrich. Polypropylene molds were obtained from TAP Plastics.

4.3.2 Preparation of SMP composites

The PU thermoset matrices were prepared from the mole ratio of TEA:HPED:HDI of 0.133: 0.4: 1. **CB5** (i.e. SMP composite containing 5wt% CB) and **CNT5** (i.e. SMP composite containing 5wt% CNT) were prepared as follows. CB and CNTs were initially dispersed in the HPED at 5wt% using a FlackTek 150 DAC speed mixer (3400 rpm, 30 sec). Next, the HPED/carbon filler dispersions were likewise sequentially blended with TEA and HDI. The final mixtures (62 mL) were cast into polypropylene molds (9 x 7 x 3 cm) and then heat treated (120°C C oven, 60 min) to initiate polymerization. The resulting specimens were removed from the molds and polished to a thickness of ~1 mm by computer numerical control (Roland MDX-540). A neat SMP control (**SMP**) was prepared as above but without introduction of carbon filler.

Prior to coating with silicone, the SMP composites were cut into 25 x 3 x 1 mm specimens using a CO_2 laser cutter (Gravograph 40 W LS100). To permit dip coating, the specimens were suspended (in the y-direction) by one end of a polypropylene rod with a small amount of epoxy glue. The other end of the rod was inserted into the holes of a custom made polycarbonate circular plate which could support up to ten rods. The top side of the circular plate was attached to a motion controller (Newport ESP3000). Al_2O_3-filled silicone was prepared by mixing Part A and Part B (50:50 wt%) with the

high speed mixer (3400 rpm, 30 sec). The silica-filled silicone was prepared by dissolving in hexane (45:55 wt%) overnight with stirring with a Teflon covered magnetic stir bar. Specimens were dip coated into the designated silicone by dipping at a rate of 2 mm/min (into the silicone), holding for 2 min, and finally removing at a rate of 2 mm/min; the entire process was lastly repeated one time. The resulting Al_2O_3-filled silicone-coated specimens (**CB5/silicone-$_{Al2O3}$** and **CNT5/silicone-$_{Al2O3}$**) were cured in an oven (90°C) for 2 hr. The resulting silica-filled silicone-coated specimens (**CB5/silicone-$_{silica}$** and **CNT5/silicone-$_{silica}$**) were sequentially cured at room temperature (RT) for 1 hr and at 70°C for 6 hr. After curing, the specimens were removed from the rods and epoxy glue was carefully applied to seal the end of the specimen.

Free-standing silicone membranes (**silicone-$_{Al2O3}$** and **silicone-$_{silica}$**) were prepared by casting the aforementioned Al_2O_3-filled silicone mixture and silica-filled silicone solution (10 mL) into molds (9 x 7 x 3 cm) and curing as above.

4.3.3 Gross appearance

Gross images of all specimens were obtained with a ProgRes digital camera (Jenoptik) attached to Leica MZ16 stereomicroscope.

4.3.4 Resistivity

The electrical resistivity of **CB5 and CNT5** (i.e. uncoated SMP composites) were compared to that of **SMP** as follows. Rectangular specimens (30 x 5 x 2 mm) were machined using Gravograph 40 W LS100 CO_2 laser machining instrument. Resistivity

was measured with a four-point probe SP4 (Signatone) apparatus equipped with an Agilent 34401A multimeter, Agilent 34420A micro-ohm meter, and Agilent E3632A DC power supply.

4.3.5 Scanning electron microscopy (SEM)

Scanning electron microscopy (SEM) was used to evaluate the morphological features of the specimens as well as silicone membrane thickness. Uncoated (i.e. **SMP**, **CB5**, **CNT5**) and **silicone-coated** (i.e. **CB5/silicone-$_{Al2O3}$**, **CNT5/silicone-$_{Al2O3}$**, **CB5/silicone-$_{silica}$** and **CNT5/silicone-$_{silica}$**) specimens were dried under vacuum at 90°C for 12 hr. Cross-sections were prepared by cutting with a clean razor blade. Surface and cross-sectional specimens were subjected to gold sputter coating (Ted Pella 6002) and viewed with a JEOL Neoscope JCM-5000 SEM at an accelerating voltage of 15 kV. The thicknesses of the Al_2O_3-filled silicone and silica-filled silicone membranes coated on SMP composites were obtained from cross-sectional SEM images. For a given coated composite, five specimens were cut in half with a clean razor blade. The resulting 10 cross-sectional surfaces were each subjected to SEM and thickness measured at three different designate areas.

4.3.6 Thermal gravimetric analysis (TGA)

TGA (TA Instruments Q50) was performed on **SMP**, **CB5**, **CNT5**, **silicone-$_{Al2O3}$** and **silicone-$_{silica}$**. Specimens (~10 mg) were placed in platinum pans and heated under

N_2 at a flow rate of 60 cm^3/min. The sample weight was recorded while the temperature was increased 10°C/min from 30 and 800°C.

4.3.7 Contact angle

The static contact angle (θ_{static}) of distilled/DI water droplets at the surface-air interface were measured by a CAM200 (KSV Instruments) goniometer equipped with an autodispenser, video camera, and drop-shape analysis software. A sessile drop of water (5-µL) was measured at 15 sec following deposition via needle onto the specimen surface. For **SMP**, **CB5**, **CNT5**, **silicone-$_{Al2O3}$** and **silicone-$_{silica}$**, the reported values are an average of three measurements taken on different areas of the same specimen.

4.3.8 Water absorption

The water uptake by **SMP**, **CB5**, **CNT5**, **silicone-$_{Al2O3}$** and **silicone-$_{silica}$** was measured gravimetrically. Specimens (5 x 5 x 1 mm) were weighed (W_i) and then immersed into 37°C deionized (DI) water bath for 0.5, 2, 6, 24, 48, 96, and 192 hr. At a designated time point, each specimen was removed from the water bath, blotted with a Kim Wipe and immediately weighed (W_f). Water absorption was quantified in terms of wt ratio of water, defined as:

$$weight\ ratio\ water\ (\%) = \left[\frac{W_f - W_i}{W_f}\right] x\ 100 \qquad (18)$$

For each specimen type, five measurements were completed.

4.3.9 Differential scanning calorimetry

T_g was determined via differential scanning calorimetry (DSC, TA Instruments Q200). First, T_g was monitored as a function of conditioning time in a 37°C deionized (DI) water bath. At designated time points (0.5, 2, 6, 24, 48, 96, and 192 hr), specimens of **SMP**, **CB5**, **CNT5**, **CB5/silicone-$_{Al2O3}$**, **CNT5/silicone-$_{Al2O3}$**, **CB5/silicone-$_{silica}$** and **CNT5/silicone-$_{silica}$** were collected, placed in hermitically sealed pans with a pin-hole punch through the top lid (for moisture evaporation) and heated from -40 to 150°C at 10°C /min. Second, specimens conditioned for 192 hr in a 37°C DI water bath were subjected to cyclic DSC experiments and T_g recovery measured. Specimens likewise placed into DSC pans and sequentially heated (10°C/min) from -40°C to a specified temperature, held isothermally for 2 min, cooled to -40ºC, and held isothermally for 2 min. A given specimens was subjected to 7 consecutive heating cycles to 70, 90, 110, 130, 150, 170, and 190°C, with each subsequent cycle employing the next highest temperature in the series.

4.3.10 Peel test

The peel strength of the silicone membranes coated onto the SMP composites was measured with a pull-off adhesion tester (DeFelsko PosiTest AT). Silicone-coated composites (**CB5/silicone-$_{Al2O3}$**, **CNT5/silicone-$_{Al2O3}$**, **CB5/silicone-$_{silica}$** and **CNT5/silicone-$_{silica}$**) (9 x 7 x 1 cm) were placed inside a mold (9 x 7 x 3 cm). Next, the aforementioned Al_2O_3-filled silicone compound and silica-filled silicone solution (10 mL) were poured on top of the designated specimens residing in the molds. Five

aluminum dollies (circular base, 10 mm diameter) were immediately set onto the uncured silicone layer of each specimen. Finally, the silicones were cured (so as to affix the dollies to the specimen) using the designated conditions previously described. The peel strength was measured before and immediately after soaking the each of the final test specimens (i.e. coated composite bearing five affixed dollies) in a 37°C DI water bath for 192 hr. A cylindrical actuator connected to a hydraulic pump was used to produce a pulling force until the dolly separated from the specimen. Reported results are based on the average of the five tests conducted on a single specimen.

4.3.11 Shape recovery

Specimens (25 x 3 x 1 mm) of **SMP**, **CB5**, **CNT5**, **CB5/silicone-$_{Al2O3}$**, **CNT5/silicone-$_{Al2O3}$**, **CB5/silicone-$_{silica}$** and **CNT5/silicone-$_{silica}$** were heated to 110°C ($T > T_g$) and then immediately deformed into a temporary U-shape to approach an initial bending angle (θ_i) of 175~180°. The temporary shape was then fixed by equilibrating the specimens at RT ($T < T_g$). Next, the specimens were immersed in a 37°C DI water bath for 0.5, 2, 6, 24, 48, 96, and 192 hr to measure the recovery of the original, permanent shape. The recovery angle (θ_r) images were recorded by a ProgRes digital camera (Jenoptik) attached to Leica MZ16 stereomicroscope. The shape recovery is expressed as:

$$\%Recovery = \left[\frac{\theta_i - \theta_r}{\theta_i}\right] x\ 100 \quad (19)$$

4.4 Results and discussion

4.4.1 Resistivity and SEM

The gross appearance of the neat PU thermoset SMP, composites and silicone-coated composites are shown in figure 4.1(a). While the presence of Al_2O_3 filler in the silicone renders it white and opaque, the silica-filled silicone is transparent. Resistivity measurements showed that **SMP** was insulating (10^{12} Ω.cm) whereas **CB5** (10^3 Ω.cm) and **CNT5** (10^2 Ω.cm) were semiconducting. The resistivity of the composites is attributed to the formation of a percolating network of carbon filler [97]. SEM images of **CB5** (figure 4.1(b)) and **CNT5** (figure 4.1(c)) reveal the presence of CB and CNT, respectively. Representative cross-sectional images of silicone-coated composites specimens are shown in figure 4.1(d) and (e). Due to the nature of the dip coating process, the silicone membrane formed an oval surface over the rectangular SMP composite. The surface and cross-sectional features are unique to the Al_2O_3-filled silicone coating (figure 4.1(f) and (h)) and silica-filled silicone membranes (figure 4.1(e) and (i)). Notably, the higher level of filler for the Al_2O_3-filled silicone is quite apparent.

The thicknesses of the silicone membranes coated on top of the SMP composites are reported in table 4.1. Due to the resultant oval geometry, thickness was determined from measurements at three distinct regions (per table 4.1). The thickest portion of the membrane (representing the longest dimension of the specimen) was ~680 μm and ~530 μm for Al_2O_3-filled and silica-filled silicone, respectively. Perpendicular to this, membrane thickness was ~280 μm and ~220 μm, respectively. Finally, the thinnest membrane dimensions were found adjacent to the corner of the enclosed rectangular

composite specimen. Here, the dimensions were ~65 µm and ~110 µm for Al_2O_3-filled and silica-filled silicone, respectively. Thickness variations at different locations as well as differences between silicone membrane types may be attributed to the differences in competing forces (e.g. surface tension, evaporation, and capillary forces) associate with the dip coating process.[98]

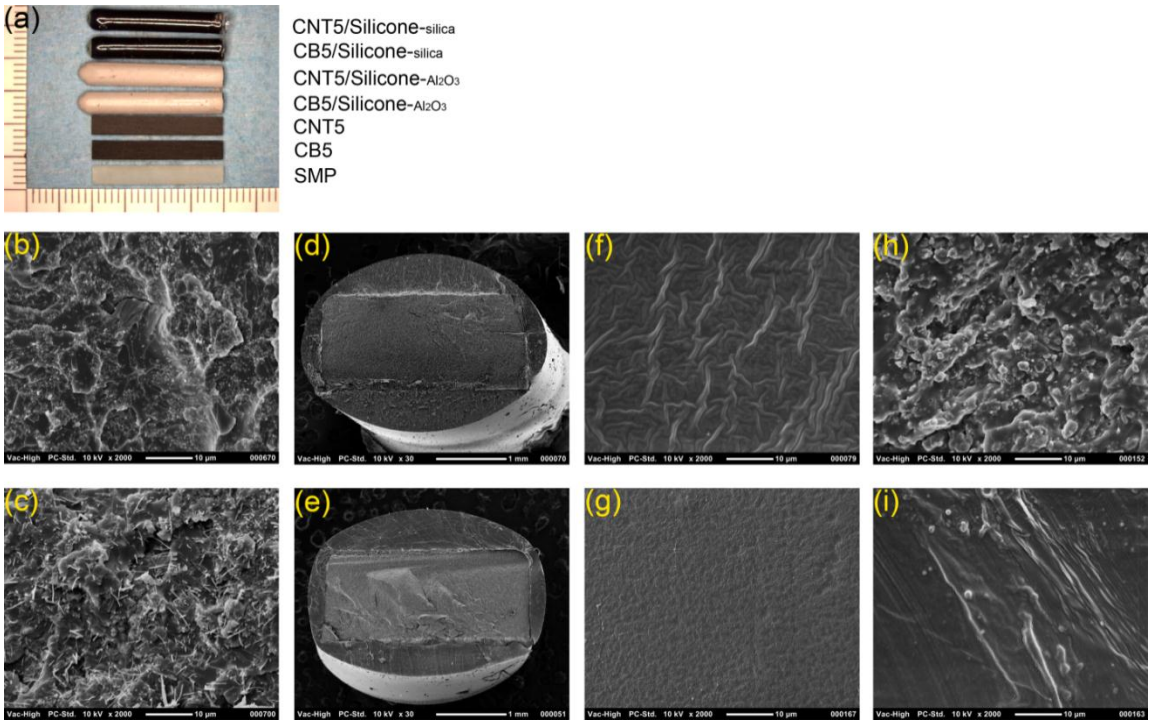

Figure 4.1 (a) Gross images of specimens (bottom to top): **SMP** (i.e. neat SMP); **CB5** and **CNT5** (i.e. SMP composite loaded with 5wt% CB and CNT, respectively); **CB5/silicone-$_{Al2O3}$, CNT5/silicone-$_{Al2O3}$, CB5/silicone-$_{silica}$ and CNT5/silicone-$_{silica}$)** (i.e. silicone-coated composites). SEM images of: (b) **CB5** cross-section; (c) **CNT5** cross-section; (d) **CB5/silicone-$_{Al2O3}$** cross-section; (e) **CB5/silicone-$_{silica}$** cross-section; (f) **silicone-$_{Al2O3}$** surface; (g) **silicone-$_{silica}$** surface; (h) **silicone-$_{Al2O3}$** cross-section; (i) **silicone-$_{silica}$** cross-section

Table 4.1 Comparison of coating membrane thickness.

	Maximum thickness		
	Side A (μm)	Side B (μm)	Corner (μm)
CB5/silicone-Al_2O_3[a]	687 ± 54	285 ± 38	64 ± 39
CNT5/silicone-Al_2O_3[b]	675 ± 38	280 ± 29	68 ± 28
CB5/silicone-silica[c]	534 ± 37	225 ± 26	108 ± 35
CNT5/silicone-silica[d]	526 ± 49	216 ± 15	116 ± 43

[a] **CB5** coated with Al_2O_3-filled silicone
[b] **CNT5** coated with Al_2O_3-filled silicone
[c] **CB5** coated with silica-filled silicone
[d] **CNT5** coated with silica-filled silicone

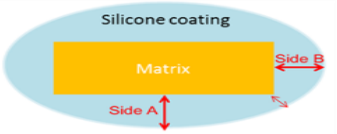

4.4.2 TGA

Thermal decomposition of the neat SMP (**SMP**) began at ~260°C and produced an anticipated negligible char (figure 4.2). Because of the inclusion of thermally stable filler [99], the decomposition of **CB5** and **CNT5** was slightly increased versus that of **SMP**. The presence of ~5wt% char for **CB5** and **CNT5** confirms the incorporation of 5wt% of CB and CNT, respectively, into the SMP matrix. The observed high thermal stability of the silicone membranes (**silicone-$_{Al2O3}$** and **silicone-$_{silica}$**) is typical of that of cured silicone networks [100]. The presence of 70% and 20% char for **silicone-$_{Al2O3}$** and **silicone-$_{silica}$**, respectively, is consistent with their known quantities of Al_2O_3 and silica.

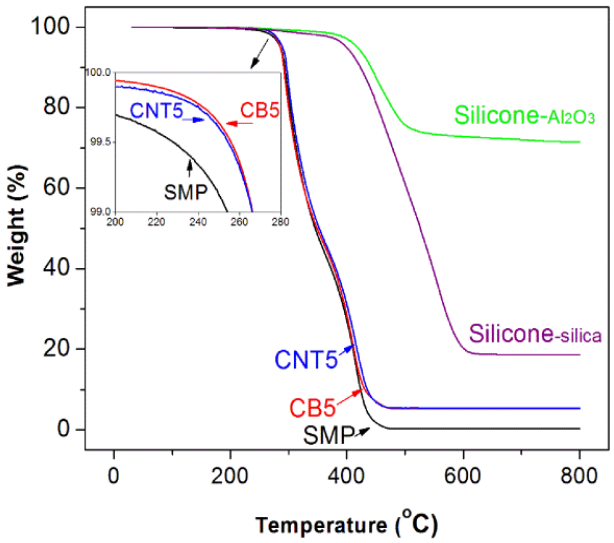

Figure 4.2 TGA of **SMP** (i.e. neat SMP); **CB5** and **CNT5** (i.e. SMP composite loaded with 5wt% CB and CNT, respectively); **silicone-$_{Al2O3}$** and **silicone-$_{silica}$** (i.e. silicone membrane only).

4.4.3 Contact angle analysis

Contact angle analysis was used to assess wettability (table 4.2). Generally, a hydrophobic surface is characterized by $\theta_{static} \geq 90$ º [101]. The neat PU thermoset SMP (**SMP**) exhibited a fairly hydrophilic surface (θ_{static} = ~79 º). Due to the addition of hydrophobic fillers, **CB5** and **CNT5**, were notably more hydrophobic (θ_{static} = ~117 and ~135º, respectively). The somewhat greater hydrophobicity of **CNT5** may be associated with the surface roughening effect associated with CNT fillers [102, 103]. As expected for crosslinked silicones [93, 94], the membranes (**silicone-$_{Al2O3}$** and **silicone-$_{silica}$**) were very hydrophobic, exhibiting θ_{static} values of ~122 and ~117º, respectively.

Table 4.2 Contact angle measurements.

SMP	**CB5**	**CNT5**	**Silicone-Al_2O_3**	**Silicone-silica**
θ_{static} (^{o})	θ_{static} (^{o})	θ_{static} (^{o})	θ_{static} (^{o})	θ_{static} (^{o})
78.7 ± 2.8	117.3 ± 6.4	135.4 ± 12.8	121.7 ± 3.2	116.8 ± 1.8

4.4.4 Water Absorption

Due to its hydrophilicty, the neat PU thermoset SMP (**SMP**) exhibited substantial water absorption, even after only 0.5 hr exposure to DI water (37°C) (figure 4.3). Between 0.5 and 192 hr of exposure, the wt% ratio of water continued to increase considerably from ~1.7 to 5%. In the case of uncoated composites **CB5** and **CNT5**, due the presence of the hydrophobic carbon fillers, the uptake of water was somewhat dimished relative to **SMP**. At all time points, the wt% ratio of water for **CB5** and **CNT5** were similar to one another and reached a maximum value of ~3.5% at 192 hr. Due to their appreciable hydrophobicity, both **silicone-$_{Al2O3}$** and **silicone-$_{silica}$** membranes exhibited a lack of measurable water uptake even after 192 hr.

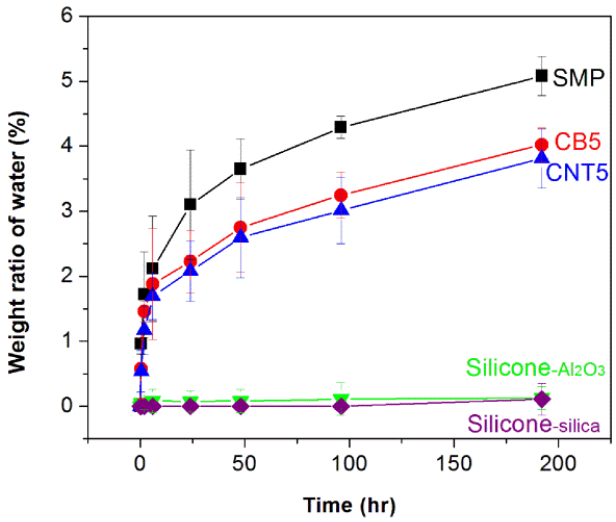

Figure 4.3 Weight % ratio of water (37°C) for **SMP** (i.e. neat SMP); **CB5** and **CNT5** (i.e. SMP composite loaded with 5wt% CB and CNT, respectively); **silicone-$_{Al2O3}$** and **silicone-$_{silica}$** (i.e. silicone membrane only).

4.4.5 Different scanning calorimetry

For the neat SMP, composites and silicone-coated composites, the depression of the T_g (of the thermosett PU SMP) was determined as a function of conditioning time in a 37°C water bath (figure 4.4). For all specimen types, the T_g was ~71°C prior to conditioning. Due to the plasticizing effect of the absorbed water, the T_g of the neat SMP (**SMP**) decreased substantially from ~71°C to ~60°C during the first 6 hr of exposure. **CNB** and **CNB** showed only a slight lessening of the T_g depression during this period. In contrast, due to the presence of a hydrophobic silicone membrane, **CB5/silicone-$_{Al2O3}$**, **CNT5/silicone-$_{Al2O3}$**, **CB5/silicone-$_{silica}$** and **CNT5/silicone-$_{silica}$** exhibited a much smaller change in T_g. Notably, T_g depression was the most diminished for composites coated with the silica-filled silicone. Thus, while water absorption could not be detected

gravimetrically (figure 4.3), a small amount of water is able to diffuse through the silicone membranes. The superior resistance of the silica-filled silicone may be attributed to its lower filler content versus the Al_2O_3-filled silicone. Upon continued conditioning, the T_g values of all specimens continued to decrease. However, the silicone membrane delayed the depression of T_g to a value of 37°C or lower verus that of uncoated composites.

Based on data reported in figures 4.3 and 4.4, T_g was plotted as a function of weight ratio of water for **SMP**, **CB5** and **CNT5** (figure 4.5). Since water uptake could not be determined for silicone-coated composites, these were not likewise analyzed. For **SMP**, a marked decrease in T_g occurs between 2% and 4% weight ratio of the water. Notably, for **CB5** and **CNT**, the decrease of T_g values with similar weight ratios of water is more substantial. Yang *et al* [82] previously demonstrated that, when the water content of the system is sufficiently high, carbon fillers tend to lower the T_g value of a thermoplastic PU SMP versus the unfilled SMP.

In a previous study, Yang *et al* [104] demonstrated that thermal cycling of a thermoplastic PU SMP previously conditioned in water can produce a recovery of the T_g due to dehydration. Thus, specimens previously conditioned in water for 192 hr were immediately subjected 7 consecutive heating cycles to in the order of 70, 90, 110, 130, 150, 170, and 190°C (figure 4.6). When cycled to 70 and 90°C, there was only a small increase in T_g values. However, T_g values substantially increased when cycled to 110, 130 and 150 ^{o}C. This is attributed to effective drying (i.e. water evaporation) of the specimens. When cycled to 170°C, there was only a small increase in T_g values,

indicating that specimens were already appreciably dehydrated. Finally, in the final heating cycle to 190°C, T_g values remained essentially unchanged, indicating that they were fully dehydrated. These final values are similar to their initital T_g values prior to conditioning (figure 4.4).

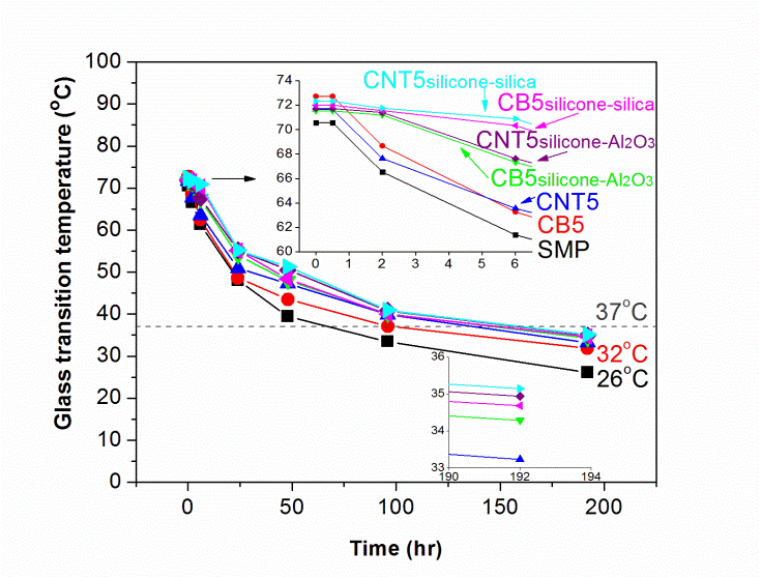

Figure4.4 T_g vs. immersion time in a 37 °C water bath for **SMP** (i.e. neat SMP); **CB5** and **CNT5** (i.e. SMP composite loaded with 5wt% CB and CNT, respectively); and **CB5/silicone-$_{Al2O3}$, CNT5/silicone-$_{Al2O3}$, CB5/silicone-$_{silica}$ and CNT5/silicone-$_{silica}$** (i.e. composites coated with silicone membrane). (T = 37ºC marked with dash line).

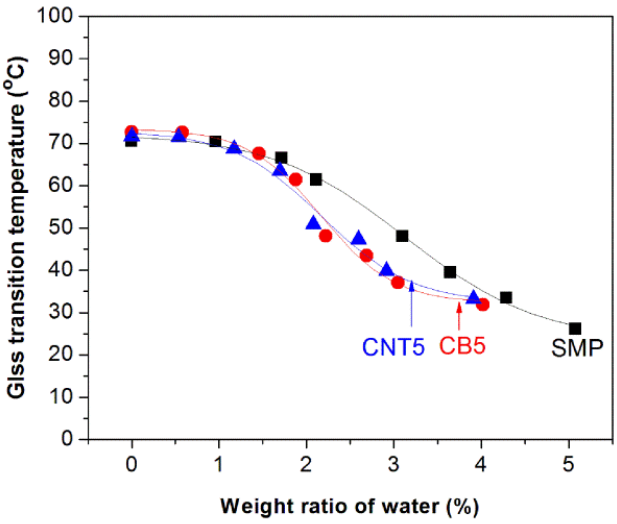

Figure 4.5 T_g as a function of weight ratio of water.

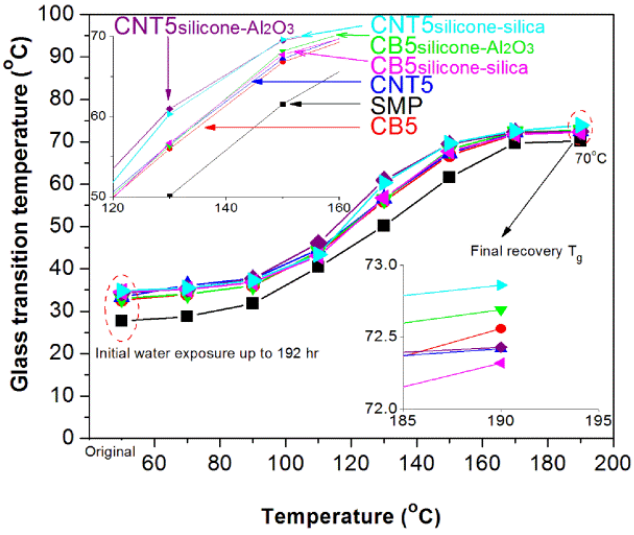

Figure 4.6 Recovery of T_g as a function of thermal cycling.

4.4.6 Peel test

Peel tests were conducted to measure the peel strength of silicone membranes to the underlying composites before and after conditioning in a 37°C water bath for 192 hr (figure 4.7). Prior to conditioning, peel strength was appreciably greater for the composites coated with the Al_2O_3-filled silicone versus the silica-filled silicone. However, after conditioning, the peel strength was only slightly higher for the Al_2O_3-filled silicone-coated composites. As noted, while water uptake cannot be measured gravimetrically for silicone-coated composites (figure 4.3), the depression of T_g at 192 hr (figure 4.4) demonstrates that water is able to slowly diffuse through the membrane and weaken bonding but without inducing delamination.

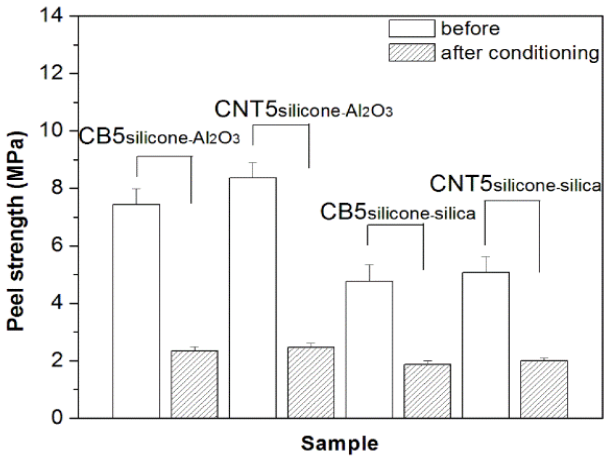

Figure 4.7 Peel strength of silicone membrane to **CB5** and **CNT5** composites before and after condition in a 37ºC water bath for 192 hr.

4.4.7 Shape recovery

The ability of specimens to retain their temporary fixed shape was measured a % recovery as a function of time conditioned in 37°C water (table 4.3). Shape recovery is predicted to increase as water uptake increases due to the subsequent decrease in T_g (from ~71°C) which serves as the T_{trans} for shape recovery. Per figure 4.8, specimens were fixed in a temporary U-shape geometry and % recovery of the permanent linear geometry by exposure to 37°C water measured at designated time points. Prior to conditioning, all specimens exhibited no shape recovery (i.e. perfect shape fixity). At 0.5 hr, **SMP** already exhibited appreciable % recovery, whereas % recovery was somewhat reduced for **CB5** and, particularly, for **CNT5**. In contrast, essentially no recovery was noted for composites coated with a silicone-membrane. At 6 hr, % recovery for **SMP** was 12% whereas that of **CB5** (9.4%) and **CNT5** (7.3%) were somewhat lower. The corresponding silicone coated composites displayed even lower % recovery values with the lowest value observed for **CNT5/silicone$_{\text{-silica}}$** (4.3%). Notably, % recovery was somewhat reduced for a given composite coated with a silica-filled silicone membrane versus an Al_2O_3-filled silicone. For these early stages of conditioning ($\leq$ 6 hr), the lack of appreciable shape recovery is consistent with the minimal depression of T_g depression due to a reduction in water absorption (figure 4.4). At 24, 48 and 96 hr, % recovery increased substantially for all specimens with the highest observed for **SMP** (44.6, 89.2 and 99%, respectively) and the lowest for **CNT5/silicone$_{\text{-silica}}$** (17.4, 64.6 and 86.5%, respectively). Again, the extent of shape recovery coincides with the trends in water uptake and depression of T_g. For instance, at 96 hr, recovery is quite

significant (~ 87 – 99%) for all specimens. This coincides with the depression of the T_g values close to that of 37°C (figure 4.4). By 192 hr, all specimens displayed 100% recovery.

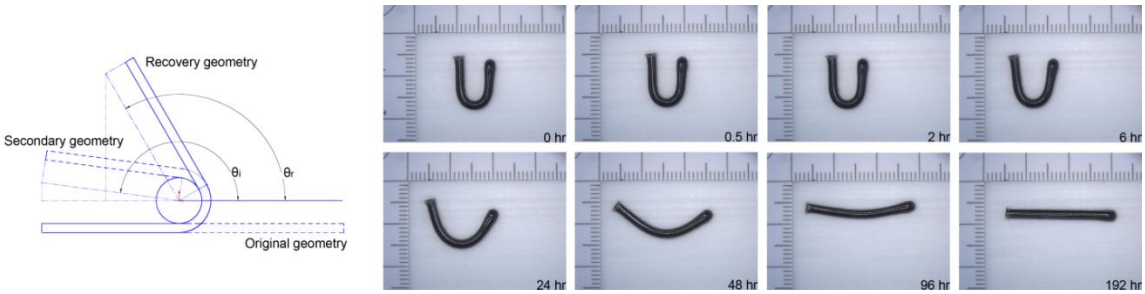

Figure 4.8 Shape recovery of **CB5**/silicone-silica as a function of exposure time to 37°C water.

Table 4.3 Shape recovery percent ratio vs. immersion time in 37°C Water.

	Shape recovery ratio							
	0 hr	**0.5 hr**	**2 hr**	**6 hr**	**24 hr**	**48 hr**	**96 hr**	**192 hr**
	(%)	*(%)*	*(%)*	*(%)*	*(%)*	*(%)*	*(%)*	*(%)*
SMP	0	3.6	7.1	12	44.6	89.2	99.0	100
CB5	0	0.8	1.9	9.4	37.8	82.6	98.2	100
CNT5	0	0.4	1.6	7.3	21.2	72.9	90.0	100
CB5/silicone-Al_2O_3	0	0.1	1.6	7.6	29.8	71.3	92.6	100
CNT5/silicone-Al_2O_3	0	0	1.0	5.7	19.6	67.6	87.2	100
CB5/silicone-silica	0	0	1.3	6.5	25.3	66.0	91.4	100
CNT5/silicone-silica	0	0	0.8	4.3	17.4	64.6	86.5	100

4.5 Conclusions

In this study, SMP composites were prepared based on a thermoset PU matrix and CB and CNT fillers and coated with an Al_2O_3- or silica-filled silicone membrane. For the neat SMP (**SMP**) and SMP composites (**CB5** and **CNT5**), water uptake (37°C) and the subsequent depression of T_g (from ~ 71°C) was substantial during early periods of conditioning (≤ 6 hr). However, particularly the silica-filled silicone membrane, substantially reduced early stage water absorption. As conditioning continued to 192 hr, the T_g values all specimens, included coated composites, were decreased substantially due to water uptake and plasticization. The impact of T_g (i.e. T_{trans}) depression on the ability to fix the temporary shape was quantified by measuring shape recovery versus time conditioning in 37 ^{o}C water. During early stages of conditioning (≤ 6 hr), the silicone membranes (particularly the silica-filled silicone) diminished shape recovery. After this, all specimens demonstrated a significant increase in shape recovery until reaching completion at 96 - 192 hr. Thus, due to the ability to prevent water absorption and T_g depression during early stages, silicone-coated electroactive SMP composite-based devices may afford the opportunity to facilitate controllable implantation (i.e. delivery and positioning within the body) by diminishing shape recovery prior to application of an electrical current. The retention of the "water-actuated" shape recovery in later stages may further facilitate functionality of the device.

CHAPTER V

MAKING AN ELECTRICAL RESISTIVE HEATING DEVICE

5.1 Overview

In order to qualify varying specimens' heating rates with different voltages and distances between inserted wires heated by DC power supply. Also, to develop an electrical resistive heating prototype to demonstrate the sequence of foam expansion from crimped secondary geometry to expanded primary geometry.

5.2 Introduction

Numerous SMPs-based devices are currently being investigated. One PEEK-based SMP suture anchor, Morphix®, has been already admitted by the FDA in 2009 and is currently implanted into patients' bodies [105]. Yakacki *et al* [66] developed the acylated-based SMP of cardiovascular stent. Lendlein *et al* [17] synthesized biodegradable SMP suture. However, the low thermal conductivity of neat SMP limited their biomedical application, such as minimally invasive surgery because of the design challenge in limited space in actuating the device by external energy. Adding inorganic fillers, higher thermal conductivity, into matrix could actuate the device from deformed shape to original shape by electrical resistive heating [18]. The previous studies of electrical resistive heating of SMP composites focused on thermoplastic urethane-based SMP with different carbon fillers [6, 25, 26, 106], and commercial thermoset styrene-based SMP resin (CRG Industries, Veriflex®) with different carbon fillers [5, 56-58, 74,

107]. In our lab, for treating brain aneurysm, we deliver the crimped thermoset SMP foam and actuate it within the aneurism [85, 108].

Cerebral aneurysms are localized dilations in the wall of a cerebral artery that is weak in structure because of thin arterial walls can cause them to rupture [109]. Surgical clipping and endovascular coils are two current options for aneurysm treatments [110]. However, surgical clipping is an invasive surgery and sometimes the aneurysm's location is inaccessible for the surgeon [111]. For endovascular coils, there are several drawbacks such as coil compaction, subsequent formation of new side aneurysms, and low packing volume leading to recanalization [108]. Our lab develops shape memory polymer foams to replace the current treatments. The crimped shape memory polymer (SMP) foam is inserted into a catheter, which is then delivered into the cerebral aneurysm by catheter and expanded by external energy, such as heat, to fill the aneurysm and prevent rupture [85].

The original design of a resistive heated device in our lab in the figure 5.1, it indicated to coil the metal wire around a rod that acts as a resistive heating device, and then the SMP foam is mounted on top of it. We then crimp the SMP foam in a tight cylindrical shape around the coiled rod. Finally, we deliver this crimped SMP foam and actuate it within the aneurism. However, sometimes when actuating by heating, uncontrollable overheating may melt the foam resulting in unfavorable results while detaching. Thus, we will use the thermoset urethane-based SMP composites with carbon particles doping to be our resistive heating device replacing the original coil resistive heating design. Also, before making this demonstration electrical resistive heating

device, fixed dimension rectangular specimens with two inserted metal wires (with varying distances between them) were heated by DC power supply. In order to determine the relationships among the different distances between inserted wires and varying voltages, the heating rate, heat temperature generation, and power generation were measured to quantify the data.

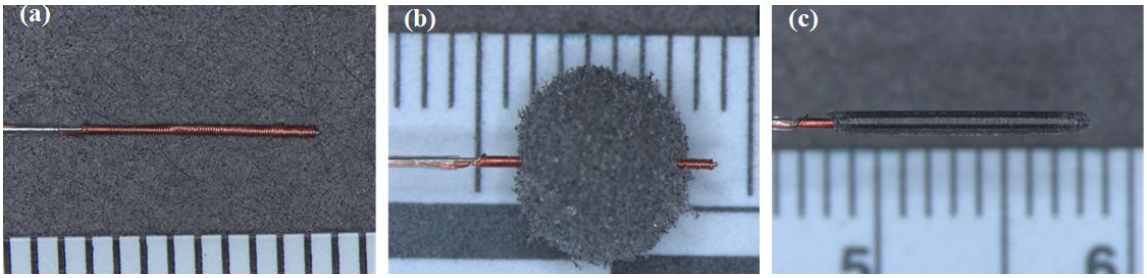

Figure 5.1 (a) Fabricated resistive heat device, (b) Mounted with SMP foam, (c) Crimped SMP foam.(Pictures from Wonjun Hwang)

5.3 Experimental

With the design goal of creating an electrical resistive heating device for minimally invasive surgery, our specimen will only require a small distance between two metal wires to generate heat by applying voltage (Agilent 6209B DC power Supply). The SMP composite specimens with loading 5wt% CB and 4.5wt% CNT were machined into 10 x 10 x 2 mm and were completely inserted with two metal wires (diameter is 0.5 mm) in the longer side. The distance between the two inserted metal wire edges was set to 1, 2, and 3 mm. The temperature was recorded by Infra-Red Camera (FLIR

ThermaCAM SC 500). Also, we calculated the relationship of current-voltage curve and of the heat temperature-power generation curve.

The SMP composites with doping weight ratio of 4.5% CNT were in the device matrix. The device size was 10 mm in length and 850 μm in diameter. The inner structure with two inserted metal wires was 127 μm in diameter separately. The device matrix used the injection method to generate the final cylinder geometry. For the assembling process, the diameter of foam was 5 mm in diameter and 10 mm in length. The SMP foam was assembled with the electrical resistive heating device and then crimped with a crimper. Finally, using a power source supplied a constant voltage to actuate the crimped foam.

5.4 Results and discussion

SMP sample with two inserted metal wires, the distance between metal wire edges is 1, 2, and 3 mm as shown in figure 5.2. Also, CB5 sample and CNT4.5 sample were heated by different voltages and heating temperature generation was recorded by IR camera for 180 seconds (figure 5.3). Figure 5.4(a) showed that the highest temperature of heat generation recorded by IR camera is a function of time. Figure 5.8 shows the maximum temperature measured on each sample at different time points. It can be seen that the maximum temperature present on the sample increases with time. Applying voltage 60 V and 80 V on the CB5 sample generated temperatures of 90 to 110°C and from 110 to 120°C, respectively. However, when applying 40 V, the

temperature stayed at around 30°C for 180 seconds. A similar trend was also shown in figure 5.4(b). Applying 40 V, 60 V, and 80 V on the CNT sample heated the sample to around 80, 95 and 110°C, respectively. Although heat generation by applying 20 V is higher than room temperature, the heat temperature is still lower than the sample's glass transition temperature. Also, the plots indicated that the sample temperature stabilized to a plateau after around 80 seconds for CB5 and around 50 seconds for CNT4.5. Both composites showed that the 1 mm distance between two inserted wires generated heat faster than either 2 mm or 3 mm. The plots of current-voltage curve of CB5 sample and of CNT 4.5 samples are shown in figure 5.5. The definition of voltage is equal to current multiplied by the resistance. An increase in resistance follows along with an increase in the distance between metal wires. The CB5 sample increased in resistance by around one order of magnitude when the distance between inserted wires increased from 1 mm to 3 mm. However, for CNT 4.5 sample, the resistance increased only slightly when compared to the CB5 sample. In figure 5.6, the plot indicated the relationship between heating temperature and power generation. The definition of power is equal to current squared multiplied by the resistance. The power generated by the CB5 sample as it was heated up to 110-120^{o}C was more than 0.025 watts. The power generated by the CNT4.5 sample as it was heated from 40^{o}C up to 120^{o}C was 0.1 to 0.3 watts. Neither power curves of CB5 nor CNT4.5 samples are linear. Thus, a shorter distance between metal wires and a higher voltage would generate higher power. In our results, we could easily change the heating temperature by changing the voltage and the distance between metal wires. In figure 5.7(a), it shows the diagram of the electrical resistive heater with foam.

Also figure 5.7(b) shows the prototype of the electrical resistive heater with crimped foam. With the demonstration of foam expanding, the electrical resistive heater with crimped foam was heated by DC power supply (figure 5.8). The sequence time of foam expansion was recorded at 0, 5, 10, 15, 20, and 25 seconds.

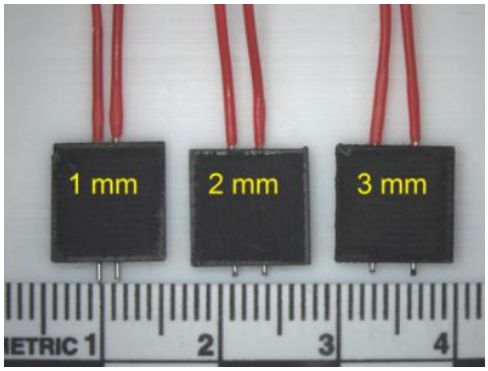

Figure 5.2 SMP sample with two inserted metal wires.

(a) 40 V for CB5 sample

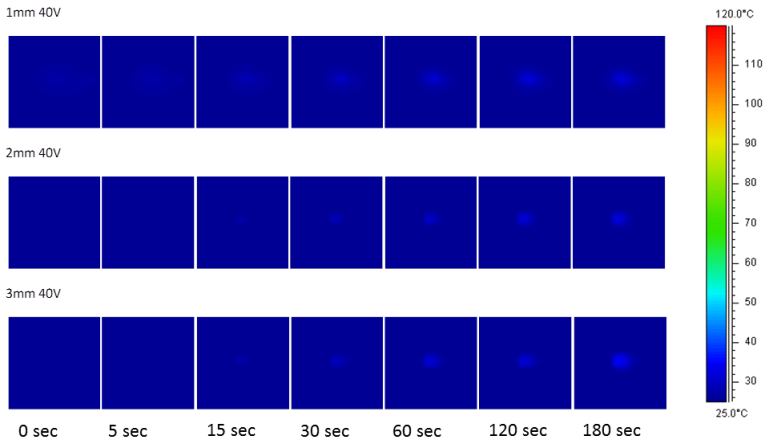

Figure 5.3 SMP sample with different distances, 1mm, 2mm, and 3mm, between two inserted metal wires heated by DC power supply.

(b) 60 V for CB5 sample

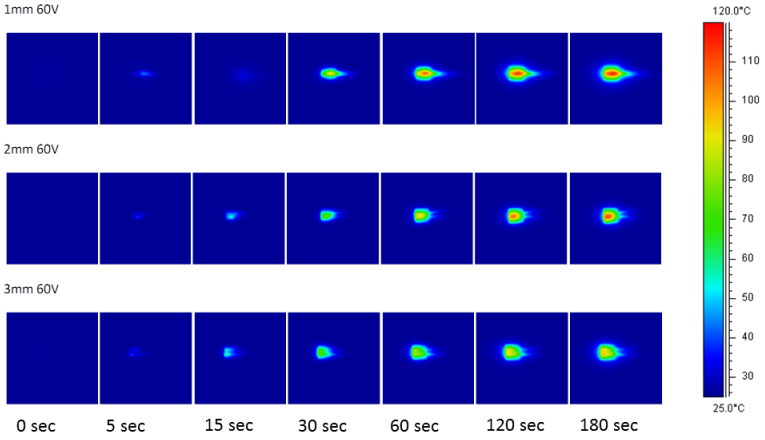

(c) 80 V for CB5 sample

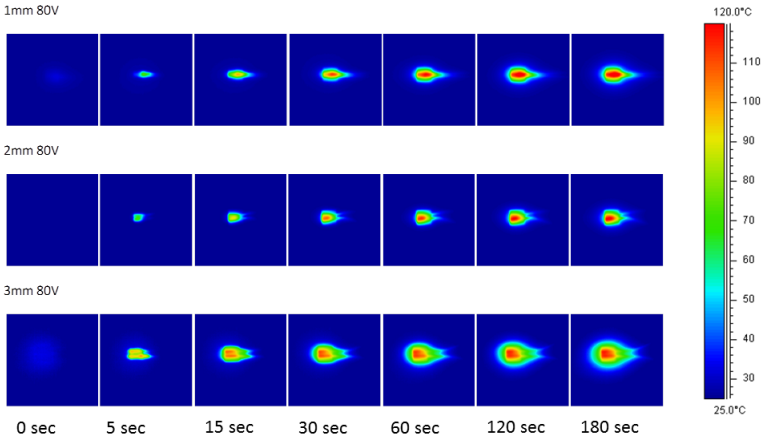

Figure 5.3 Continued.

(d) 20 V for CNT4.5 sample

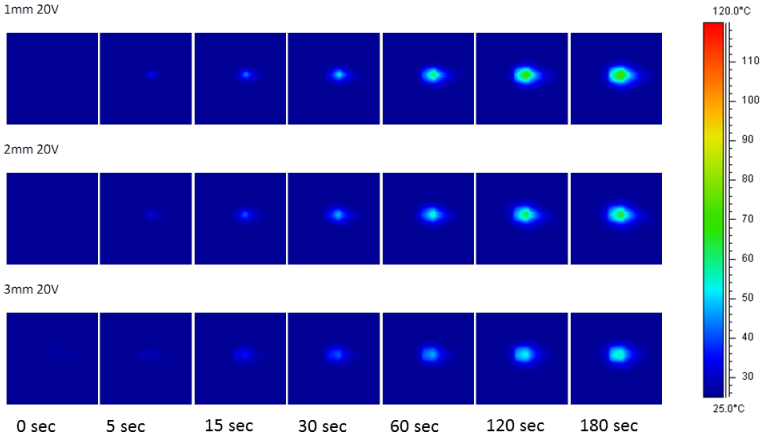

(e) 40 V for CNT4.5 sample

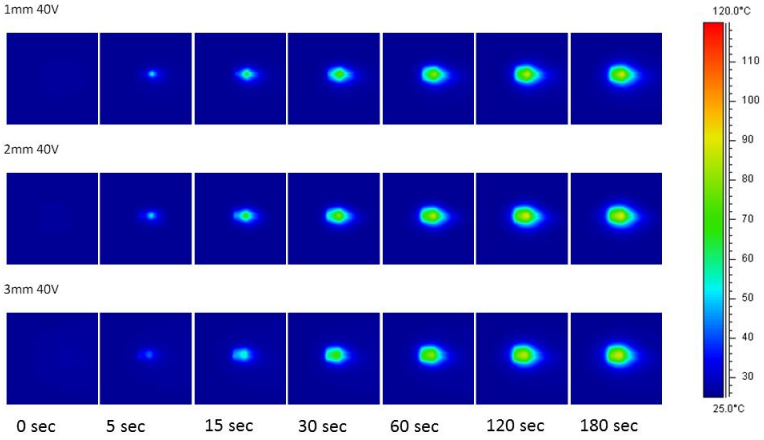

Figure 5.3 Continued.

(f) 60 V for CNT4.5 sample

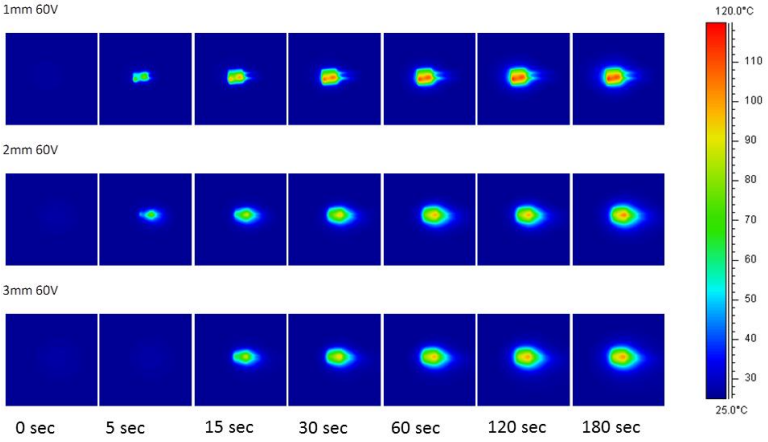

(g) 80 V for CNT4.5 sample

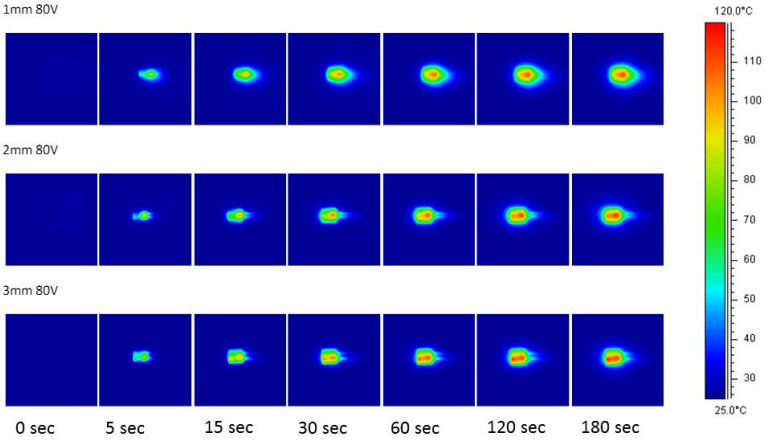

Figure 5.3 Continued.

(a)

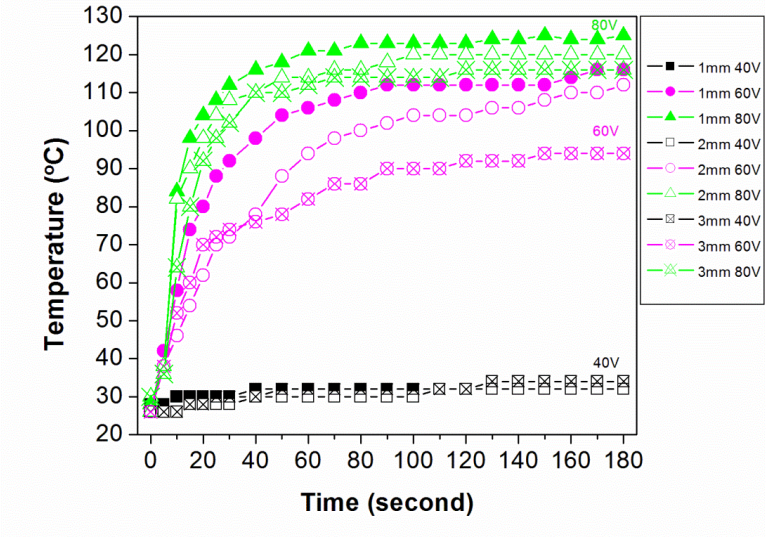

(b)

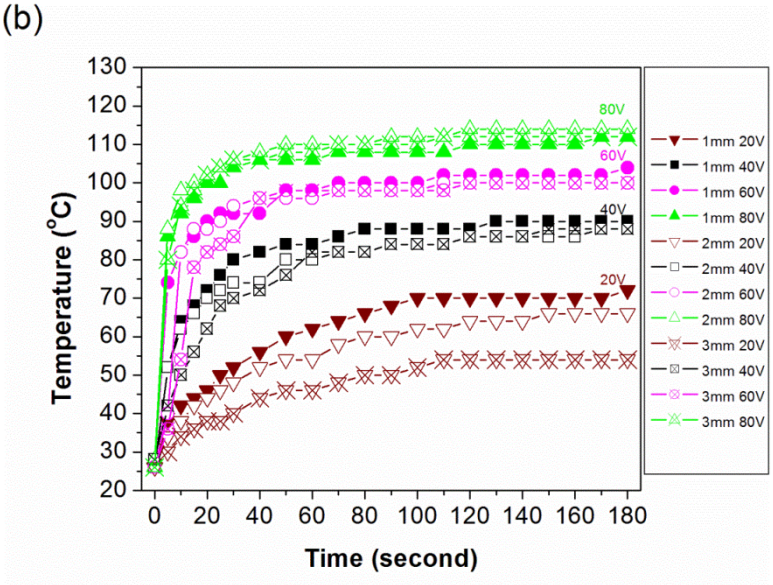

Figure 5.4 Electrical resistive heating generated by different voltage and different distance between insert metal wires: (a) CB5; (b) CNT4.5.

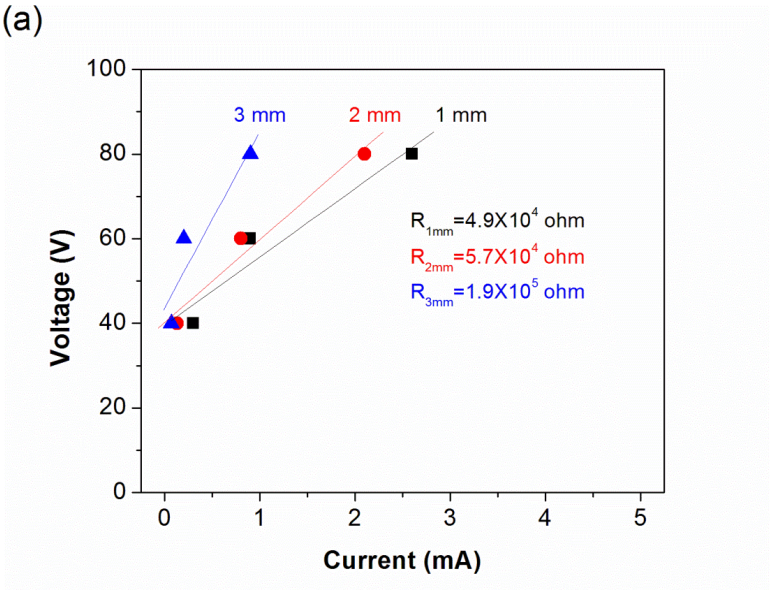

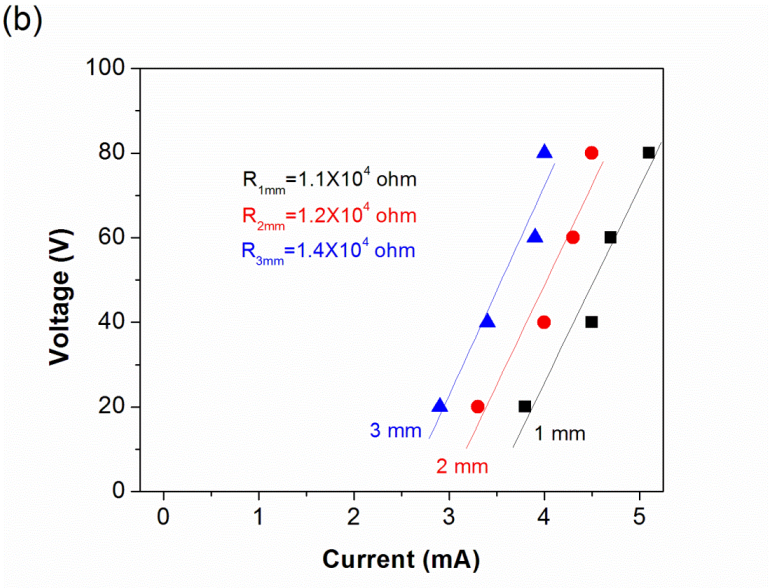

Figure 5.5 The plots of current-voltage curve: (a) CB5; (b) CNT4.5.

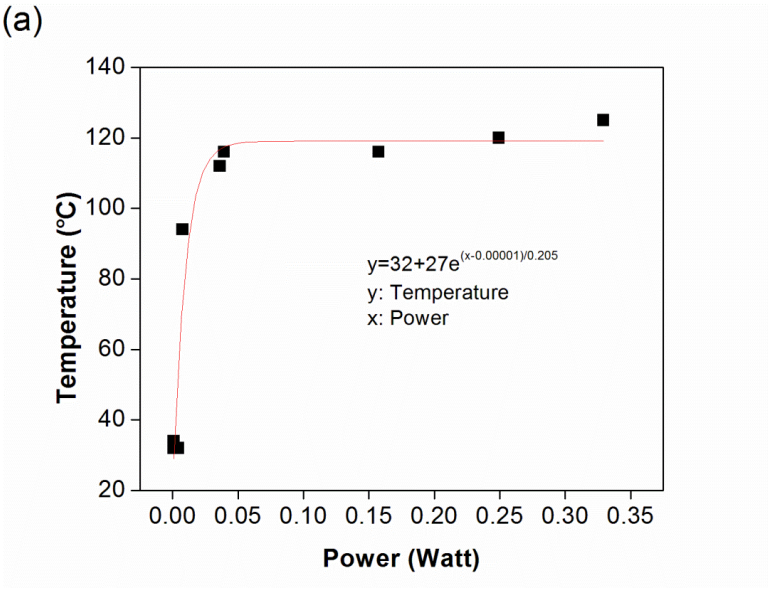

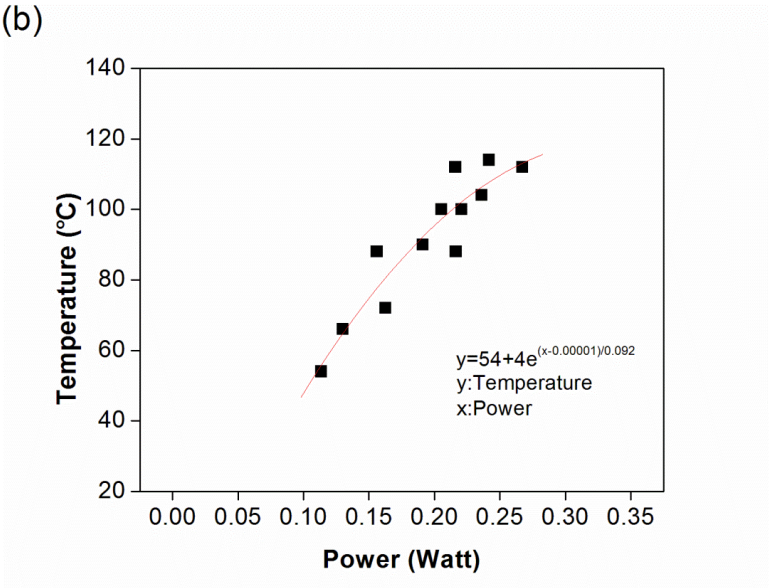

Figure 5.6 The relationship between heating temperature and power generation: (a) CB5; (b) CNT4.5.

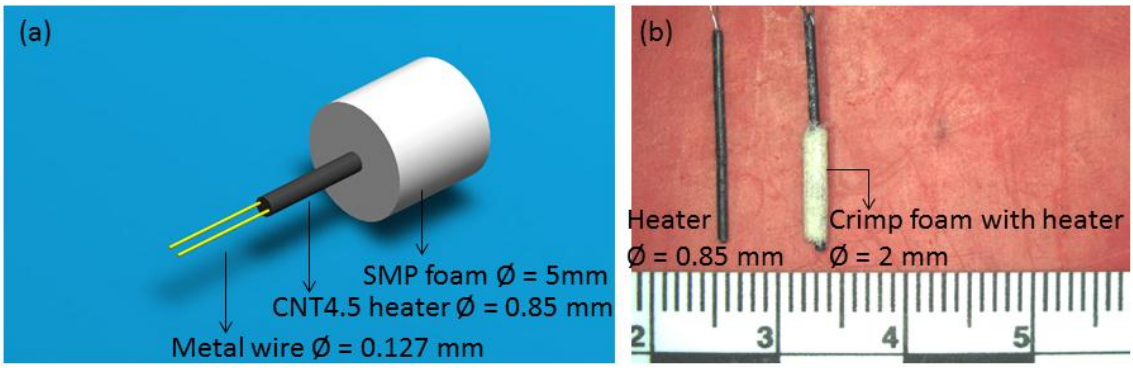

Figure 5.7 (a) The diagram of electrical resistive heater with foam; (b) The prototype electrical resistive heater with crimped foam.

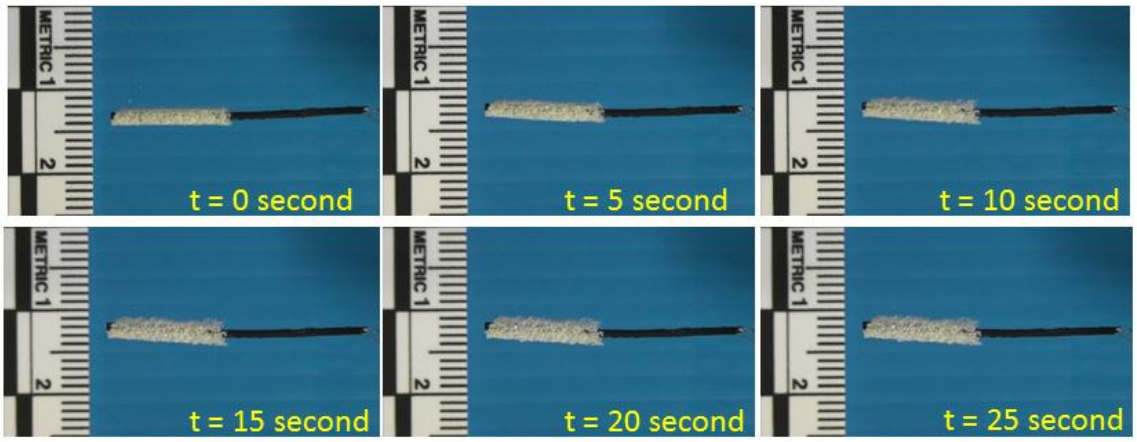

Figure 5.8 Sequence of foam expanding from electrical resistive heating with crimped foam.

5.5 Conclusions

Higher resistive heat and faster heating rate are related to an increase in power supply and the decrease in distance between the inserted metal wires. Research conducted on carbon fillers within SMP thermoset matrices has the potential for the material to be self-actuated upon application of a voltage, which makes this research advantageous for electrical resistive heating of device design.

CHAPTER VI

CONCLUSIONS

This study is focused on the thermoset urethane-based SMP composites with CB and CNT fillers and the evaluation of their thermomechanical behavior, electrical properties, water absorption rate, and quantifying the effectiveness of the resistive heating device. The dispersion percentage of the fillers in the SMP composites with CB are around 95-98% and with CNT they are around 80-84%. Increasing filler concentration lowered the Tg, increased the glassy and rubbery moduli, and increased the recovery stress. Compared to CB loading, CNT loading resulted in both a higher modulus and recovery stress increase along with a more significant decrease in recoverable strain capacity. The electrical percolation threshold of the SMP composites was approached at loading CB fillers around 3-4wt% and loading CNT fillers around 2.5-3.5wt%. Also, due to the effect of positive temperature coefficient caused the increase in electrical resistivity and changes in electrical resistance induced by strain extension, the stable heat conductivity loads 5wt% CB fillers and 4.5wt% CNT fillers into the matrix of SMP composites to create a continuous network that enables an electron to pass through the filler freely. Tests of the shape memory recovery with both CB7 and CNT7 after applying power supply showed around an 83-88% recovery from their 180 degree secondary geometry. In the water absorption test, loading carbon filler CB5 and CNT5 into SMP composites absorbed less water when compared to NP because an increase in hydrophobicity due to the fillers. Also, the silicone-membrane coating also lowers the water absorption rate due to the hydrophobic coating. For the

shape memory recovery in 37^{o}C water, all specimens were bent into 180 degree secondary shape and then recovered into their original straight shape after 192 hr. Quantifying the electrical resistive heating of the device with loading CNT4.5 filler provided a faster heating rate compared to the loading of CB5 filler. Lastly, a higher resistive heat generation is related to an increase in power supply and to a decrease in distance between the inserted metal wires.

REFERENCES

[1] Liu C, Qin H and Mather P T 2007 Review of progress in shape-memory polymers *J. Mater. Chem.* **17** 1543-58.

[2] Sun L, Huang W M, Ding Z, Zhao Y, Wang C C, Purnawali H and Tang C 2012 Stimulus-responsive shape memory materials: A review *Mater. Des.* **33** 577-640.

[3] Behl M and Lendlein A 2007 Shape-memory polymers *Mater. Today* **10** 20-8.

[4] Huang W M, Yang B, Zhao Y and Ding Z 2010 Thermo-moisture responsive polyurethane shape-memory polymer and composites: a review *J. Mater. Chem.* **20** 3367-81.

[5] Leng J S, Huang W M, Lan X, Liu Y J and Du S Y 2008 Significantly reducing electrical resistivity by forming conductive Ni chains in a polyurethane shape-memory polymer/carbon-black composite *Appl. Phys. Lett.* **92** 204101-3.

[6] Gunes I S, Jimenez G A and Jana S C 2009 Carbonaceous fillers for shape memory actuation of polyurethane composites by resistive heating *Carbon* **47** 981-97.

[7] Gunes I S, Cao F and Jana S C 2008 Evaluation of nanoparticulate fillers for development of shape memory polyurethane nanocomposites *Polymer* **49** 2223-34.

[8] Koerner H, Price G, Pearce N A, Alexander M and Vaia R A 2004 Remotely actuated polymer nanocomposites[mdash]stress-recovery of carbon-nanotube-filled thermoplastic elastomers *Nat. Mater.* **3** 115-20.

[9] Li F, Qi L, Yang J, Xu M, Luo X and Ma D 2000 Polyurethane/conducting carbon black composites: Structure, electric conductivity, strain recovery behavior, and their relationships *J. Appl. Polym. Sci.* **75** 68-77.

[10] Lendlein A and Kelch S 2002 Shape-memory polymers *Angew. Chem. Int. Ed.* **41** 2034-57.

[11] Lendlein A, Jiang H, Junger O and Langer R 2005 Light-induced shape-memory polymers *Nature* **434** 879-82.

[12] Sahoo N G, Jung Y C, Goo N S and Cho J W 2005 Conducting shape memory polyurethane-polypyrrole composites for an electroactive actuator *Macromol. Mater. Eng.* **290** 1049-55.

[13] Buckley P R, McKinley G H, Wilson T S, Small W, Benett W J, Bearinger J P, McElfresh M W and Maitland D J 2006 Inductively heated shape memory polymer for the magnetic actuation of medical devices *IEEE Trans. Biomed. Eng.* **53** 2075-83.

[14] Yang B, Huang W M, Li C and Li L 2006 Effects of moisture on the thermomechanical properties of a polyurethane shape memory polymer *Polymer* **47** 1348-56.

[15] Sun L, Huang W M, Ding Z, Zhao Y, Wang C C, Purnawali H and Tang C 2012 Stimulus-responsive shape memory materials: A review *Mater. Des.* **33** 577-640.

[16] Behl M, Razzaq M Y and Lendlein A 2010 Multifunctional shape-memory polymers *Adv. Mater.* **22** 3388-410.

[17] Lendlein A and Langer R 2002 Biodegradable, Elastic shape-memory polymers for potential biomedical applications *Science* **296** 1673-6.

[18] Rousseau I A 2008 Challenges of shape memory polymers: A review of the progress toward overcoming SMP's limitations *Polym. Eng. Sci.* **48** 2075-89.

[19] Gunes I S and Jana S C 2008 Shape memory polymers and their nanocomposites: A review of science and technology of new multifunctional materials *J. Nanosci. Nanotechno.* **8** 1616-37.

[20] Liang C, Malafeew E and CRogers C A 1997 Investigation of shape memory polymers and their hybrid composites *J. Intell. Mater. Syst. Struct.* **8** 380-6.

[21] Ohki T, Ni Q-Q, Ohsako N and Iwamoto M 2004 Mechanical and shape memory behavior of composites with shape memory polymer *Compos. Part A: Appl. Sci. Manuf.* **35** 1065-73.

[22] Cho J W and Lee S H 2004 Influence of silica on shape memory effect and mechanical properties of polyurethane–silica hybrids *Eur. Polym. J.* **40** 1343-8.

[23] Jimenez G and Jana S C 2007 Composites of carbon nanofibers and thermoplastic polyurethanes with shape-memory properties prepared by chaotic mixing *Polym. Eng. Sci.* **49** 2020-30.

[24] Paik I H, Goo N S, Yoon K J, Jung Y C and Cho J W 2005 Electric resistance property of a conducting shape memory polyurethane actuator *Key Eng. Mater.* **297-300** 1539-44.

[25] Cho J W, Kim J W, Jung Y C and Goo N S 2005 Electroactive shape-memory polyurethane composites incorporating carbon nanotubes *Macromol. Rapid Commun.* **26** 412-6.

[26] Jung Y C, Yoo H J, Kim Y A, Cho J W and Endo M 2010 Electroactive shape memory performance of polyurethane composite having homogeneously dispersed and covalently crosslinked carbon nanotubes *Carbon* **48** 1598-603.

[27] Iijima S and Ichihashi T 1993 Single-shell carbon nanotubes of 1-nm diameter *Nature* **363** 603-5.

[28] Iijima S 1991 Helical microtubules of graphitic carbon *Nature* **354** 56-8.

[29] Wei B Q, Vajtai R and Ajayan P M 2001 Reliability and current carrying capacity of carbon nanotubes *Appl. Phys. Lett.* **79** 1172-4.

[30] Poncharal P, Wang Z L, Ugarte D and de Heer W A 1999 Electrostatic deflections and electromechanical resonances of carbon nanotubes *Science* **283** 1513-6.

[31] Coleman J N, Khan U, Blau W J and Gun'ko Y K 2006 Small but strong: A review of the mechanical properties of carbon nanotube–polymer composites *Carbon* **44** 1624-52.

[32] Huang J-C 2002 Carbon black filled conducting polymers and polymer blends *Adv. Polym. Tech.* **21** 299-313.

[33] Bourrat X 1993 Electrically conductive grades of carbon black: Structure and properties *Carbon* **31** 287-302.

[34] Princy K G, Joseph R and Kartha C S 1998 Studies on conductive silicone rubber compounds *J. Appl. Polym. Sci.* **69** 1043-50.

[35] Tchoudakov R, Breuer O, Narkis M and Siegmann A 1996 Conductive polymer blends with low carbon black loading: Polypropylene/polyamide *Polym. Eng. Sci.* **36** 1336-46.

[36] Kirkpatrick S 1973 Percolation and conduction *Rev. Mod. Phys.* **45** 574-88.

[37] Aharoni S M 1972 Electrical resistivity of a composite of conducting particles in an insulating matrix *J. Appl. Phys.* **43**.

[38] Janzen J 1975 On the critical conductive filler loading in antistatic composites *J. Appl. Phys.* **46** 966-9.

[39] Bueche F 1972 Electrical resistivity of conducting particles in an insulating matrix *J. Appl. Phys.* **43** 4837-8.

[40] Miyasaka K, Watanabe K, Jojima E, Aida H, Sumita M and Ishikawa K 1982 Electrical conductivity of carbon-polymer composites as a function of carbon content *J. Mater. Sci.* **17** 1610-6.

[41] Sumita M, Asai S, Miyadera N, Jojima E and Miyasaka K 1986 Electrical conductivity of carbon black filled ethylene-vinyl acetate copolymer as a function of vinyl acetate content *Colloid. Polym. Sci.* **264** 212-7.

[42] Liang J and Yang Q 2007 Aggregate structure and percolation behavior in polymer/carbon black conductive composites *J. Appl. Phys.* **102** 083508-6.

[43] Berhan L and Sastry A M 2007 Modeling percolation in high-aspect-ratio fiber systems. I. Soft-core versus hard-core models *Phys. Rev. E* **75** 041120.

[44] Sahoo N G, Rana S, Cho J W, Li L and Chan S H 2010 Polymer nanocomposites based on functionalized carbon nanotubes *Prog. Polym. Sci.* **35** 837-67.

[45] Vaisman L, Wagner H D and Marom G 2006 The role of surfactants in dispersion of carbon nanotubes *Adv. Colloid Interface Sci.* **128–130** 37-46.

[46] Islam M F, Rojas E, Bergey D M, Johnson A T and Yodh A G 2003 High weight fraction surfactant solubilization of single-wall carbon nanotubes in water *Nano Lett.* **3** 269-73.

[47] Geng H-Z, Kim K K, So K P, Lee Y S, Chang Y and Lee Y H 2007 Effect of acid treatment on carbon nanotube-based flexible transparent conducting films *J. Am. Chem. Soc.* **129** 7758-9.

[48] Zhang G, Sun S, Yang D, Dodelet J-P and Sacher E 2008 The surface analytical characterization of carbon fibers functionalized by H_2SO_4/HNO_3 treatment *Carbon* **46** 196-205.

[49] Shao Y, Yin G, Zhang J and Gao Y 2006 Comparative investigation of the resistance to electrochemical oxidation of carbon black and carbon nanotubes in aqueous sulfuric acid solution *Electrochim. Acta* **51** 5853-7.

[50] Hill D E, Lin Y, Rao A M, Allard L F and Sun Y-P 2002 Functionalization of carbon nanotubes with polystyrene *Macromolecules* **35** 9466-71.

[51] Velasco-Santos C, Martínez-Hernández A L, Fisher F T, Ruoff R and Castaño V M 2003 Improvement of thermal and mechanical properties of carbon nanotube composites through chemical functionalization *Chem. Mater.* **15** 4470-5.

[52] Viswanathan G, Chakrapani N, Yang H, Wei B, Chung H, Cho K, Ryu C Y and Ajayan P M 2003 Single-step in situ synthesis of polymer-grafted single-wall nanotube composites *J. Am. Chem. Soc.* **125** 9258-9.

[53] Vondráček P and Doležel B 1984 Biostability of medical elastomers: A review *Biomaterials* **5** 209-14.

[54] Francolini I, Donelli G and Stoodley P 2003 Polymer designs to control biofilm growth on medical devices *Rev. Environ. Sci. Biotechnol.* **2** 307-19.

[55] Ikada Y 1994 Surface modification of polymers for medical applications *Biomaterials* **15** 725-36.

[56] Leng J, Lan X, Liu Y and Du S 2011 Shape-memory polymers and their composites: Stimulus methods and applications *Prog. Mater Sci.* **56** 1077-135.

[57] Leng J, Lv H, Liu Y and Du S 2007 Electroactivate shape-memory polymer filled with nanocarbon particles and short carbon fibers *Appl. Phys. Lett.* **91** 144105-7.

[58] Leng J S, Lan X, Liu Y J and Du S Y 2009 Electroactive thermoset shape memory polymer nanocomposite filled with nanocarbon powders *Smart Mater. Struct.* **18** 074003.

[59] Liu Y, Gall K, Dunn M L and McCluskey P 2004 Thermomechanics of shape memory polymer nanocomposites *Mech. Mater.* **36** 929-40.

[60] Yakacki C M, Satarkar N S, Gall K, Likos R and Hilt J Z 2009 Shape-memory polymer networks with Fe3O4 nanoparticles for remote activation *J. Appl. Polym. Sci.* **112** 3166-76.

[61] Wilson T S, Bearinger J P, Herberg J L, Marion J E, Wright W J, Evans C L and Maitland D J 2007 Shape memory polymers based on uniform aliphatic urethane networks *J. Appl. Polym. Sci.* **106** 540-51.

[62] Hearon K, Singhal P, Horn J, Small W, Olsovsky C, Maitland K C, Wilson T S and Maitland D J 2013 Porous shape-memory polymers *Polymer Reviews* **53** 41-75.

[63] Meng Q and Hu J 2009 A review of shape memory polymer composites and blends *Compos. Part A: Appl. Sci. Manuf.* **40** 1661-72.

[64] Voit W, Ware T, Dasari R R, Smith P, Danz L, Simon D, Barlow S, Marder S R and Gall K 2010 High-strain shape-memory polymers *Adv. Funct. Mater.* **20** 162-71.

[65] Yakacki C M, Shandas R, Safranski D, Ortega A M, Sassaman K and Gall K 2008 Strong, tailored, biocompatible shape-memory polymer networks *Adv. Funct. Mater.* **18** 2428-35.

[66] Yakacki C M, Shandas R, Lanning C, Rech B, Eckstein A and Gall K 2007 Unconstrained recovery characterization of shape-memory polymer networks for cardiovascular applications *Biomaterials* **28** 2255-63.

[67] Ware T, Hearon K, Lonnecker A, Wooley K L, Maitland D J and Voit W 2012 Triple-shape memory polymers based on self-complementary hydrogen bonding *Macromolecules* **45** 1062-69.

[68] Yu Y-J, Hearon K, Wilson T S and Maitland D J 2011 The effect of moisture absorption on the physical properties of polyurethane shape memory polymer foams *Smart Mater. Struct.* **20** 085010.

[69] Nicolais L and Narkis M 1971 Stress-strain behavior of styrene-acrylonitrile/glass bead composites in the glassy region *Polym. Eng. Sci.* **11** 194-9.

[70] Thostenson E T, Li C and Chou T-W 2005 Nanocomposites in context *Compos. Sci. Technol.* **65** 491-516.

[71] Gall K, Dunn M L, Liu Y, Finch D, Lake M and Munshi N A 2002 Shape memory polymer nanocomposites *Acta Mater.* **50** 5115-26.

[72] Brent L V, Dimitris C L and Duncan J M 2011 Characterizing and modeling the free recovery and constrained recovery behavior of a polyurethane shape memory polymer *Smart Mater. Struct.* **20** 094004.

[73] Yu Y-J, Hearon K, Wilson T S and Maitland D J 2011 The effect of moisture absorption on the physical properties of polyurethane shape memory polymer foams *Smart Mater. Struct.* **20** 085010.

[74] Lan X, Liu Y, Lv H, Wang X, Leng J and Du S 2009 Fiber reinforced shape-memory polymer composite and its application in a deployable hinge *Smart Mater. Struct.* **18** 024002.

[75] Schmidt A M 2006 Electromagnetic Activation of shape memory polymer networks containing magnetic nanoparticles *Macromol. Rapid Commun.* **27** 1168-72.

[76] Yu Y-J, Infanger S, Hearon K, Rodriguez J N, Chu C-C, Wilson T S and Maitland D J 2013 Thermoset shape memory polyurethane composites with carbon fillers *Smart Mater. Struct.* **submitted**.

[77] Tsang D K L, Marsden B J, Fok S L and Hall G 2005 Graphite thermal expansion relationship for different temperature ranges *Carbon* **43** 2902-6.

[78] Suárez S, Ramos-Moore E and Mücklich F 2013 A high temperature X-ray diffraction study of the influence of MWCNTs on the thermal expansion of MWCNT/Ni composites *Carbon* **51** 404-9.

[79] Kwon Y-K, Berber S and Tománek D 2004 Thermal contraction of carbon fullerenes and nanotubes *Phys. Rev. Lett.* **92** 015901.

[80] Sau K P, Chaki T K and Khastgir D 1998 The change in conductivity of a rubber-carbon black composite subjected to different modes of pre-strain *Compos. Part A: Appl. Sci. Manuf.* **29** 363-70.

[81] Pramanik P K, Khastagir D and Saha T N 1993 Effect of extensional strain on the resistivity of electrically conductive nitrile-rubber composites filled with carbon filler *J. Mater. Sci.* **28** 3539-46.

[82] Yang B, Min Huang W, Li C and Hoe Chor J 2005 Effects of moisture on the glass transition temperature of polyurethane shape memory polymer filled with nano-carbon powder *Eur. Polym. J.* **41** 1123-8.

[83] W. Small I, Singhal P, Wilson T S and Maitland D J 2010 Biomedical applications of thermally activated shape memory polymers *J. Mater. Chem.* **20** 3356-66.

[84] Singhal P, Rodriguez J N, Small W, Eagleston S, Van de Water J, Maitland D J and Wilson T S 2012 Ultra low density and highly crosslinked biocompatible shape memory polyurethane foams *J. Polym. Sci., Part B: Polym. Phys.* **50** 724-37.

[85] Ortega J, Maitland D, Wilson T, Tsai W, Savaş Ö and Saloner D 2007 Vascular dynamics of a shape memory polymer foam aneurysm treatment technique *Ann. Biomed. Eng.* **35** 1870-84.

[86] Sperling L H, *Introduction to Physical Polymer Science*, 3rd ed. (John Wiley & Sons, Inc., Canada, 2001).

[87] Kim B Y S, Rutka J T and Chan W C W 2010 Nanomedicine *N. Engl. J.Med.* **363** 2434-43.

[88] Kim S J, Lee I T, Lee H-Y and Kim Y H 2006 Performance improvement of an ionic polymer–metal composite actuator by parylene thin film coating *Smart Mater. Struct.* **15** 1540-6.

[89] Zhuang X, Nikoozadeh A, Beasley M A, Yaralioglu G, G,, Khuri-Yakub B T and L. P B 2007 Biocompatible coatings for CMUTs in a harsh, aqueous environment *J. Micromech. Microeng.* **17** 994-1001.

[90] Sun N, Qin S, Wu J, Cong C, Qiao Y and Zhou Q 2012 Bio-inspired superhydrophobic polyphenylene sulfide/polytetrafluoroethylene coatings with high performance *J. Nanosci. Nanotechno.* **12** 7222-5.

[91] Hawkins M L and Grunlan M A 2012 The protein resistance of silicones prepared with a PEO-silane amphiphile *J. Mater. Chem.* **22** 19540-6.

[92] Rushton D N, Brindley G S, Polkey C E and Browning G V 1989 Implant infections and antibiotic-impregnated silicone rubber coating *J. Neurol., Neurosurg. Psychiatry.* **52** 223-9.

[93] Hron P 2003 Hydrophilisation of silicone rubber for medical applications *Polym. Int.* **52** 1531-9.

[94] Bartzoka V, McDermott M R and Brook M A 1999 Protein-silicone interactions *Adv. Mater.* **11** 257-9.

[95] Dyke M E V, Clarson S J and Arshady R, *Silicone biomaterials. An introduction to polymeric biomaterials*. (Ed. Citus Books: London, 2003).

[96] Curtis J and Colas A, in *Biomaterials Science*, edited by Ratner B D, Hoffman A S, Schoen F J and Lemons J E (Elsevier Academic Press, San Diego, CA, 2004), pp. 697-707.

[97] Kirkpartrick S 1973 Percolation and conduction *Rev. Modern Phys.* **45** 574-88.

[98] Brinker C J, Hurd A J, Schunk P R, Frye G C and Ashley C S 1992 Review of sol-gel thin film formation *J. Non-cryst. Solids* **147-147** 424-36.

[99] Zeng J, Saltysiak B, Johnson W S, Schiraldi D A and Kumar S 2004 Processing and properties of poly(methyl methacrylate)/carbon nano fiber composites *Compos. Part B: Eng.* **35** 173-8.

[100] Dvornic P R, in *Silicon-Containing Polymers: The Science and Technology of Their Synthesis and Applications*, edited by Jones R G, Ando W and Chojnowski J (Kluwer Academic Publishers, Dordrecht, The Netherlands, 2000), pp. 200-10.

[101] Sangermano M B, R.; Malucelli, G.; Priola, A.; Pollicino, and A.; Recca A 2003 Fluorinated epoxides as surface modifying agents of UV-curable systems *J. Appl. Polym. Sci.* **89** 1524-9.

[102] Lau K K S, Bico J, Teo K B K, Chhowalla M, Amaratunga G A J, Milne W I, McKinley G H and Gleason K K 2003 Superhydrophobic carbon nanotube forests *Nano Lett.* **3** 1701-5.

[103] Hong Y C, Shin D H, Cho S C and Uhm H S 2006 Surface transformation of carbon nanotube powder into super-hydrophobic and measurement of wettability *Chem. Phys. Lett.* **427** 390-3.

[104] Yang B, Huang W M, Li C, Lee C M and Li L 2004 On the effects of moisture in a polyurethane shape memory polymer *Smart Mater. Struct.* **13** 191.

[105] Barber F A, Herbert M A and Crates J M 2013 A comparison of lateral ankle ligament suture anchor strength *Foot Ankle Surg.* **19** 108-11.

[106] Il Hyun P, Nam Seo G, Yong Chae J and Jae Whan C 2006 Development and application of conducting shape memory polyurethane actuators *Smart Mater. Struct.* **15** 1476.

[107] Liu Y, Lv H, Lan X, Leng J and Du S 2009 Review of electro-active shape-memory polymer composite *Compos. Sci. Technol.* **69** 2064-8.

[108] Rodriguez J N, Yu Y-J, Miller M W, Wilson T S, Hartman J, Clubb F J, Gentry B and Maitland D J 2012 Opacification of shape memory polymer foam designed for treatment of intracranial aneurysms *Ann. Biomed. Eng.* **40** 883-97.

[109] Currie S, Mankad K and Goddard A 2011 Endovascular treatment of intracranial aneurysms: review of current practice *Postgrad. Med. J.* **87** 41-50.

[110] Molyneux A 2002 International Subarachnoid Aneurysm Trial (ISAT) of neurosurgical clipping versus endovascular coiling in 2143 patients with ruptured intracranial aneurysms: a randomised trial *The Lancet* **360** 1267-74.

[111] Johnston S C, Zhao S, Dudley R A, Berman M F and Gress D R 2001 Treatment of unruptured cerebral aneurysms in California *Stroke* **32** 597-605.

APPENDIX

A composite material's dispersion characteristics depend on the filler loading percentage, particle size and distribution; however, until now, there has been no specific technique to quantitatively account for all three at the same time.

Dr. Khare and Dr. Burris, from the Department of Mechanical Engineering, University of Delaware, have found one way to interpret dispersion published on *Polymer* **51** 719-29. They also provided the MATLAB^{TM} code to quantify the dispersion at the following the website: http://research.me.udel.edu/~dlburris/software/. The free-space length, L_f, is defined as the length of one side of the largest theoretical square that could fit between the nearest filler particles in the polymer matrix. Figure A.1 indicates the same loading 6.5 % in the matrix under four different dispersions. In practice, a smaller L_f was measured with more uniform filler dispersion with a constant filler loading and size. A reduced filler size for a given loading and an increased filler loading in the matrix for a given filler size would also reduce the L_f.

For sample preparation, the composite specimens were cut to 10 μm thickness and the surface morphology of SMP composites were analyzed using a Zeiss Axiovert 200 microscope. The image was converted into black (fillers) and white (matrix) to measure the free-space length. The free-space length is defined as the most probable number of intersecting fillers is zero. Initially, the free-space square with length, L, is a randomly located on the black and white image with statically significant number 1000 times. In the dispersion system, the Poisson distribution could describe the probability of intersecting fillers in the free-space square. The probability density is defined as $f(k,\lambda)=e^{-\lambda}\lambda^k/k!$ where f is the probability, k is the actual number of occurrences and λ is

the expected number of occurrences. The procedure is shown in figure A.2. For a length of 100 μm, the most probable number of fillers per square shows high occurrence signals; this means that any length larger than the above value results in no filler-free domain. For a length of 10 μm, the most probable number of fillers per square is 0; the free-space length can be no smaller than 10 μm, meaning that any smaller free-space squares do not contain fillers. Finally, this method indicated that the free-space length of 1wt% CB in the SMP matrix is 25.1 ± 0.7 μm with 3 images measurements.

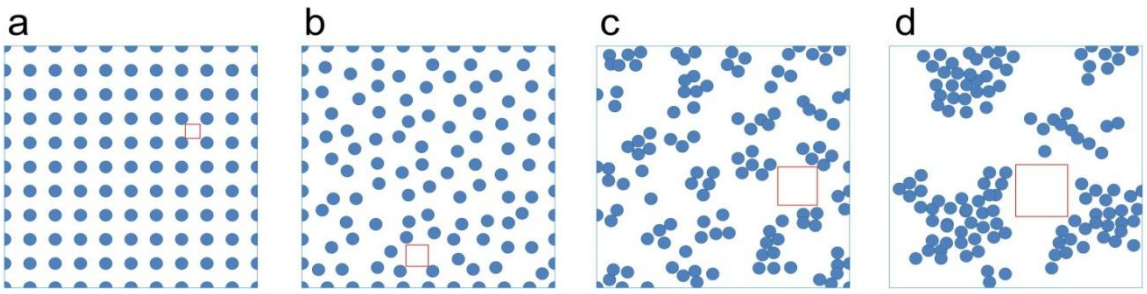

Figure A.1 Varying dispersion of 1 μm fillers at 6.5% loading in the image size 20 x 20 μm: (a) uniform dispersion, L_f = 1.1 μm; (b) random dispersion, L_f = 1.5 μm; (c) clustered dispersion, L_f = 3.0 μm; (d) agglomerated dispersion, L_f = 4.4 μm. Open squares with red color have a length equal to free-space length, L_f.

Agglomerates could also follow the same concept and procedure as above for calculating the agglomeration length, L_a. Agglomerates is defined as the continuous regions of fillers in the matrix. Initially, we took the above black and white image to reverse the both colors where white now represents the agglomerates of continuous fillers and black now represents the unfilled polymer matrix. Then, by following the steps above, the agglomeration length can be measured.

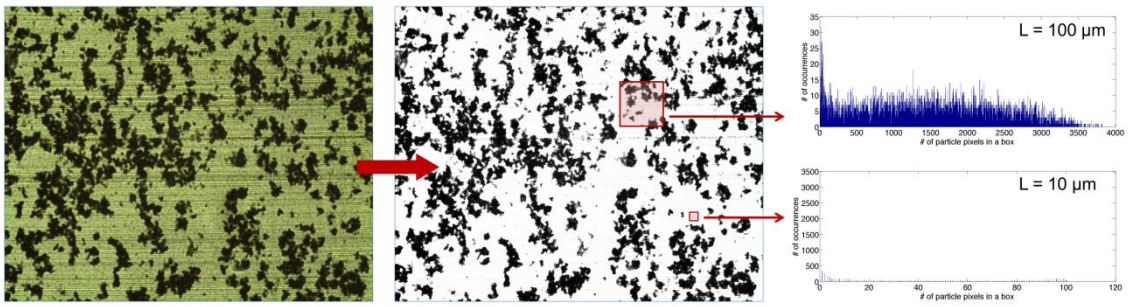

Figure A.2 Optical microscope images of the loading 1wt% CB into urethane-based SMP for calculating the free-space length. The largest square size with free-space length is that there is no occurrence of intersecting fillers in the square. (Image size is 640 x 510 µm)

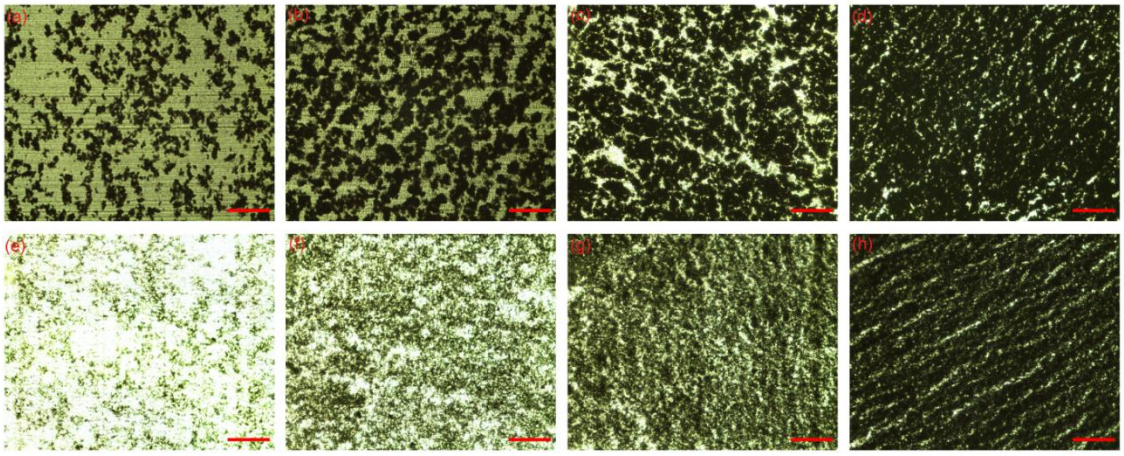

Figure A.3 Optical microscope images of the distribution of carbon fillers in the SMPs matrix: (a) CB1 is 1wt% carbon black; (b) CB3 is 3wt% carbon black; (c) CB5 is 5wt% carbon black; (d) CB7 is 7wt% carbon black; (e) CNT1 is 1wt% carbon nanotube; (f) CNT3 is 3wt% carbon nanotube; (g) CNT5 is 5wt% carbon nanotube; (h) CNT7 is 7wt% carbon nanotube (scale bar, 100 µm).

Figure A.3 shows the 10x magnification image of urethane-based SMP composites with loading 1wt%, 3wt%, 5wt%, and 7wt% of CB and CNT separately. All

images are converted into black and white, and then we computed their free-space length. With increasing filler loading, the free-space length of SMP composites with loading CB fillers decreases from 25 to 3 μm, and the agglomeration length of that increase from 19 to 37 μm as shown in table A.1. The same trend is also shown in the system of SMP composites with loading CNT fillers.

Table A.1. Free space length and agglomeration length of loading different wt% carbon fillers in the SMPs matrix.

Filler loading	Free space length (μm)[a]	Agglomeration length (μm)[a]
CB1	25.1 ± 0.7	18.6 ± 0.2
CB3	8.6 ± 1.2	30.2 ± 1.1
CB5	7.2 ± 0.9	31.1 ± 3.3
CB7	2.6 ± 0.4	36.5 ± 1.3
CNT1	43 ± 3.8	1.7 ± 0.1
CNT3	20 ± 2.4	6.3 ± 2.3
CNT5	6 ± 1.6	16 ± 0.6
CNT7	1.3 ± 0.4	29 ± 0.4

[a]Mean ± stand deviation (n=3)

This method is valid for any distribution of particles. We could compare the composites with the same filler loading under different preparation procedures. Also, we could discuss the relationship among the value of tensile modulus, elongation to break, free-space and agglomeration lengths for the dispersion. However, there is some limitation in this method of measuring distribution. In order to compare the free-space lengths between two different composite systems, they should always contain the same filler loading. Second, when computing the free-space length from black and white

images, they should always be chosen from the same magnification image. For example, the figure A.4 shows the optical microscope images of 3wt% CB in the SMPs matrix with different magnification 10x and 20x. The free-space length of the same filler loading with different magnification images is 8.6 ± 1.2 μm and 18.7 ± 3.7 μm separately. Thus, the free-space length of CB3 SMP composites of 20x magnification image is 2.2 times larger than 10x one.

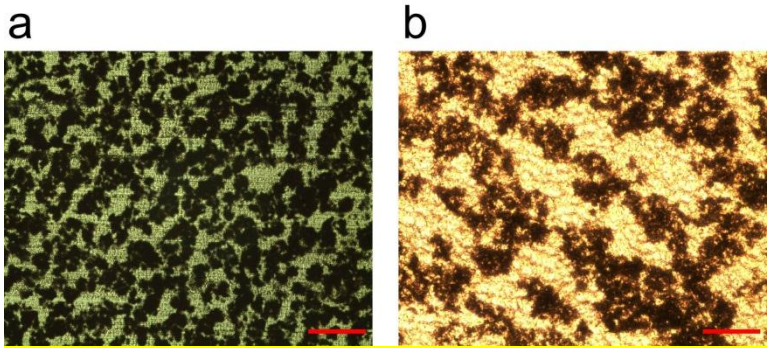

Figure A.4 Optical microscope images of 3wt% CB in the SMPs matrix: (a) 10x magnification (scale bar = 100 μm); (b) 20x magnification (scale bar = 35 μm).